Rev.Adv.Mater.Sci. 11 (2006) 19-45

BEAMS OF ATOMIC CLUSTERS: EFFECTS ON IMPACT WITH SOLIDS

V.N. Popok and E.E.B. Campbell

Department of Physics, Göteborg University, 41296 Göteborg, Sweden

Received: May 12, 2005

Abstract. A state-of-the-art review in the field of cluster beams and energetic cluster-surface interaction is presented. Ionised cluster beams are considered to be a controllable and versatile tool for modification and processing of surfaces and near-surface layers on an atomic scale as an alternative to ion implantation, ion assisted deposition and some other methods. A brief introduction to the history of cluster beams is given as well as a discussion of the capabilities of cluster beams for a variety of applications in material science, electronics and optics. Techniques for producing atomic and molecular clusters are described. Energetic cluster deposition and cluster implantation as well as related physical effects are the main emphasis of the review. In the final part of the paper the attention is focused on the study of surface erosion (crater formation) under energetic cluster ion impact.

1. INTRODUCTION

Atomic (or molecular) clusters are aggregates of a few up to tens of thousands of atoms (or molecules) that show properties intermediate between those of individual atoms (or molecules), with discrete energy states, and bulk matter characterised by continua or bands of states. More detailed information about the classification of clusters, their bonding types and structure goes beyond the scope of this review and can be found elsewhere [1,2].

Cluster beams can be tools for manipulating agglomerates of atoms providing the synthesis of structures on the nm-scale. In particular, one can control the cluster (nanoparticle) size, its impact energy and, to a certain extent, the spatial distribution of the deposited nanoparticles on a surface, for example, by preliminary processing or functionalisation [3]. Finite size effects can lead to electronic, optical, magnetic and other properties that are quite different from those of molecules or condensed matter and that can be of great interest for practical applications in nanotechnology [4-9]. With clusters consisting of up to thousands of atoms it is possible to transport and locally deposit a large amount of material, providing an advanced method for growth of thin films which can be either porous or very compact and smooth depending on the energy regime used for cluster impact [10,11]. Low-energy cluster implantation is found to be an efficient tool for doping of shallow layers with suppression of dopant diffusion during post-implantation annealing [12]. Cluster beams can also be used as very efficient tools for processing of surfaces (dry etching and cleaning) or improving their surface topology (smoothing) [13]. Current achievements in the application of cluster beams are summarised in the next section.

Corresponding author: V.N. Popok, e-mail: popok@physics.gu.se

2. BRIEF HISTORY AND PRESENT-DAY APPLICATIONS OF CLUSTER BEAMS

The first mention of cluster beam production and investigation occurred at the end of the 50's and beginning of the 60's [14,15]. The possibility to separate small clusters of hydrogen, nitrogen and argon from non-condensed residual gas and transfer them into a high vacuum was shown. At the same time it was demonstrated with CO_2 and H_2 that cluster beams can be ionised by electron bombardment enabling mass spectra to be obtained [15,16]. These experiments were followed by investigations of the cluster size distribution in a beam of $(CO_2)_n^+$, depending on conditions of the cluster source [17] and by development of methods to evaluate cluster sizes, for example, by scattering of a potassium atomic beam passing through a nitrogen cluster beam [18]. Slightly later, first studies on the reflection of molecular nitrogen clusters from polished stainless steel, showing a strong maximum at 90° reflection angle independent of the angle of incidence, were carried out [19]. At the beginning of the 70's, experiments on the stopping of swift proton clusters in carbon and gold foils were performed [20]. The use of accelerated ionised clusters for practical applications has been pioneered by the Kyoto group. In the 70's they reported the development of a cluster source for ionised-cluster beam deposition [21]. However, first published results on the deposition of Si, Au, and Cu suffer from a lack of confirmation concerning the cluster-to-monomer ratio in the beams. Further development of the technique in the 80's provided more controllable parameters of the beams and showed the applicability of ionised clusters for synthesis of thin metal films and heterostructures [22,23]. However, no clear picture of the physical background emerged until the beginning of the 90's when systematic experimental work corroborated by molecular dynamic simulations on thin film growth by energetic cluster deposition was published by the Haberland group, see for example [10,24,25].

One of the important parameters in the practical application of cluster beams is impact energy. By varying the cluster energy from low values (below or on the level of eV/atom), corresponding to soft-landing of a cluster on the surface, to high values (keV-MeV/atom) suitable for implantation one can develop a variety of methods for synthesis and modification of materials.

A large amount of mass and energy can be deposited locally when using charged clusters, forming compact and almost atomically smooth films. This approach became of increasing interest in the late 90's with intensive development of sub-micron and nano-electronics. For example, growth of good-quality Ge layers with a thickness of 100-400 nm on a Si substrate at a temperature of 500 °C, which is lower than the critical temperature of epitaxial growth by molecular beams or CVD, was reported by using a germanium cluster beam at supersonic velocities [26]. Silicon films with tuneable photoluminescence properties were synthesised by low-energy deposition of size-selected Si clusters (Fig. 1); the obtained characteristics were well described in terms of zero-dimensional quantum dots [27]. By deposition of neutral carbon clusters it was possible to grow nanostructured graphite-like films and patterns of three-dimensional objects using a mask (Fig. 2) [28,29]. This method of formation of patterned carbon dots on the silicon surface followed by the thermal annealing was later employed to obtain arrays of SiC dots for applications in electronics [30]. Recently, deposition of pure carbon clusters from a supersonic beam provided experimental evidence for the possibility of producing a carbyne-rich pure carbon solid [31]: before this publication, the existence of carbyne was strongly debated [32]. The cluster beam deposition technique was also found to be an efficient and powerful tool for fabrication of organic (polymer) thin films and various inorganic-organic

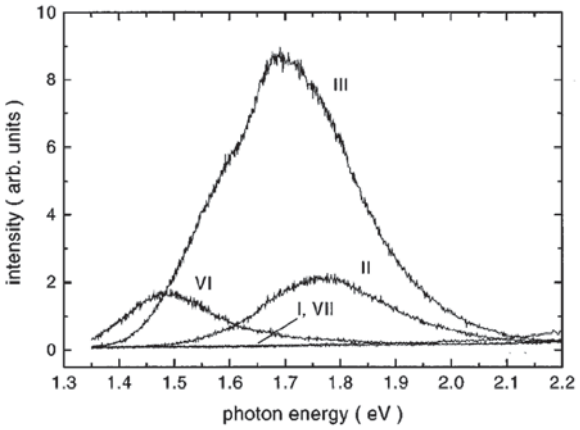

Fig. 1. Photoluminescence spectra of thin films produced by deposition of size-selected silicon nanocrystals. The 488-nm line of an argon-ion laser was used for excitation. Mean diameters of the nanocrystals are 2.47 (I), 3.65 (II), 3.92 (III), 4.95 (VI) and 6.37 (VII) nm. Reprinted with permission from [27]. Copyright 1997, American Physical Society.

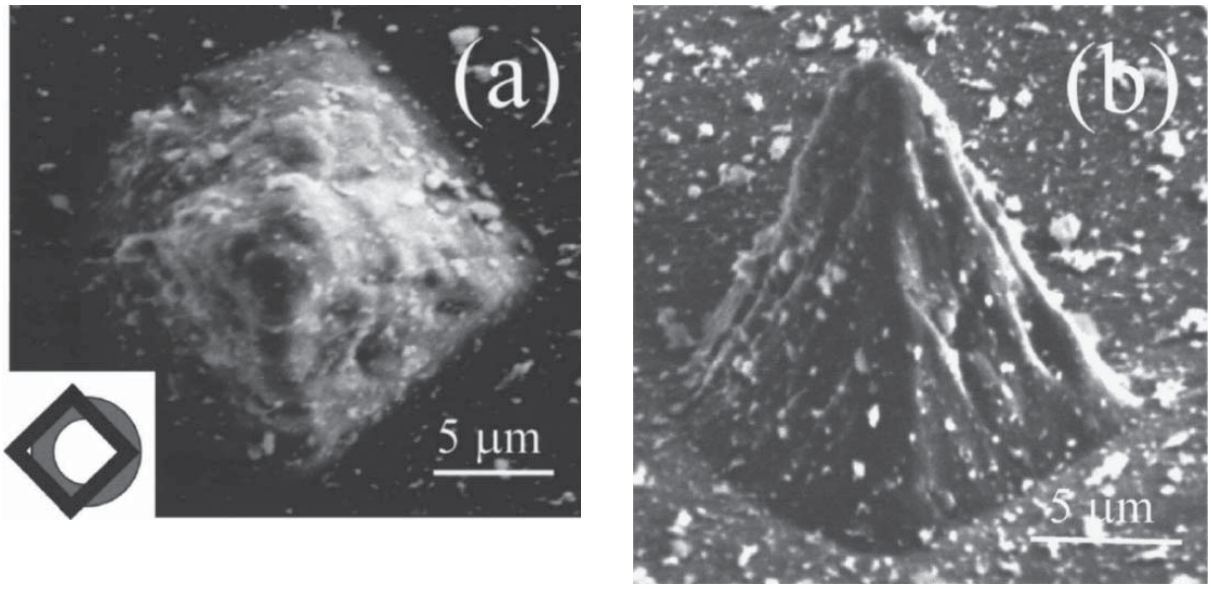

Fig. 2. SEM images of (a) vertical and (b) 60° tilted tip deposited through superposition of two grids (see insertion in panel (a)) using a carbon cluster beam. Reprinted with permission from [29]. Copyright 2000, American Institute of Physics.

complex nanometer-scale functional structures, see for example review [33]. Thus, the high deposition rates as well as the control of the energy and cluster mass distribution makes the cluster beam technique competitive with other synthetic routes for materials where a well-defined morphology and structure is required.

A promising application of the low-energy cluster beam deposition technique is the preparation of optical, magnetic, and magneto-optic nanostructures formed by clusters of various metals on the surface of a dielectric matrix [4,5]. In the case of noble metal or copper nanoparticles, the films exhibit specific absorption bands in the near-UV, visible or near-IR regions depending on the cluster species [6,7] due to the collective excitation of conduction electrons (surface plasmon resonance). The position, shape and intensity of such absorption bands strongly depend on the size distribution, shape and volumetric fraction of the metallic inclusions. In this context, the cluster beam technique offers some unique possibilities for controlling these parameters and synthesising composites with variable optical properties [34-36]. Size-controlled granular magnetic films and films of magnetic nanoparticles embedded in various matrices can be fabricated using cluster beams of transition metals (Co, Fe, Ni, *etc.*) [8,9,37-40]. This is of growing interest for applications for high-density memory devices, magnetic sensors and spin electronics.

Energetic cluster deposition, so-called pinning, when the cluster is slightly embedded into a substrate but preserves its composition gives an opportunity to prevent cluster diffusion on the surface [41]. The pinned, size-selected clusters have potential applications in many fields, such as fabrication of semiconductor nanostructures and the immobilisation and orientation of biological molecules [42]. By initial processing of a surface, for instance by focused ion irradiation, it was found to be possible to produce regular arrays of surface defects, so-called surface functionalisation, by which deposited metal clusters can be organised on the surface, giving control of the nanoparticle size, the geometry, and the periodicity of the array (Fig. 3) [3,43].

Cluster ion beam processing in conjunction with one or several other methods may provide the opportunity to realise otherwise difficult to obtain compositions or material phases. Cluster ion beam-assisted deposition has been used, for example, for the growth of high-quality, thin and smooth films of ITO [44], Ta_2O_5, Nb_2O_5 [45] and TiO_2 [46]. Ionised cluster beams with low acceleration energy are useful for preparing transparent TiO_2 thin films for the efficient photocatalytic degradation of pollutants diluted in water and air [47]. The combination of this method and metal ion (V^+, Cr^+, *etc.*) implantation can produce TiO_2 thin films that are able to operate not only under UV light but also under visible light

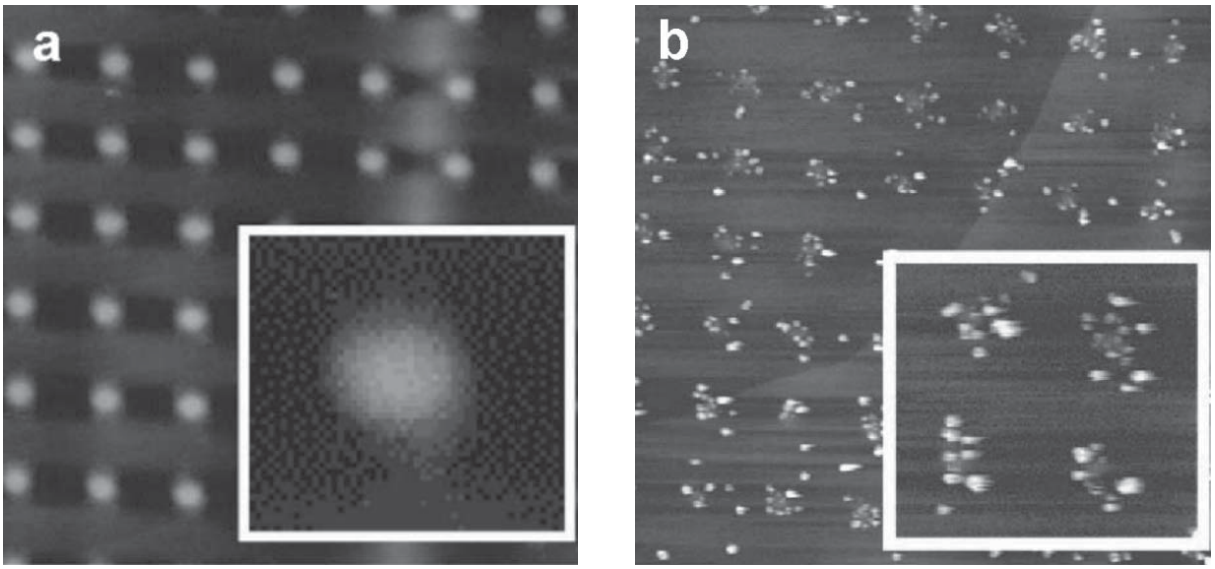

Fig. 3. AFM images (2×2 μm) of (a) defects created by focused ion beam (FIB) with a dose of 10000 ions/point on HOPG and (b) $6.7 \cdot 10^{-3}$ ML gold film deposited on FIB patterned HOPG surface with a dose of 2000 ions/point. Reprinted with permission from [43]. Copyright 2004, Elsevier.

irradiation [47]. Carbon nitride films exhibiting an extremely high hardness and low initial and steady-state friction coefficients as well as low wear rates were obtained by a reactive ionised cluster beam technique where the carbon clusters pass through a reactive gas (N_2) and the resulting particles are deposited on the substrate [48]. It was also expected that the application of nitrogen cluster beam-assisted deposition for production of materials such as cBN and C_3N_4 might yield a means to achieve compositions that were nearly impossible to obtain by other means. However, this suggestion has not been experimentally proven yet.

The use of cluster beams for shallow implantation is one of the topical applications. Implantation of silicon by chemically reactive cluster ions of $(O_2)_n^+$ and $(CO_2)_n^+$ with energies of 5-10 keV showed formation of high quality SiO_2 films of a few nm thickness that can be adaptable for fabrication of ultrathin insulating layers for semiconductor devices [49]. An advantage of the 'cluster method' is the very low surface roughness (below 0.5 nm) of the film [45] compared to so-called passive oxidation (SiO_2 formation under high oxygen pressure and high temperature) [50]. Synthesis of such thin SiO_2 films by other methods, for example, by pulsed laser deposition or plasma-enhanced chemical-vapour deposition (CVD), was found to be impossible due to either bubble formation (laser) or porous structure (CVD) resulting in poorer quality and higher roughness of the films [51,52].

Present-day technology has led to the use of lower and lower implantation energy and has moved to heavier implant species because the new generation of transistors already needs to have junctions of 30-50 nm. However, when the energy of the ion beam is reduced to a few keV, the beam current drops off due to the space-charge effect which limits the practical use of low-energy ion implantation. Recently, it was shown that low-energy implantation of $B_{10}H_{14}$ clusters is an efficient way for doping of shallow silicon layers [12,53]. The most important phenomenon found is the suppression of enhanced boron diffusion in the cluster-implanted silicon during the post-implantation thermal annealing. The physical nature of the effect is not understood yet but the phenomenon allows the doped layer as well as the junction thickness to be kept within a few nm. A transistor with a 40 nm effective gate length was fabricated by such cluster implantation (Fig. 4). This size is comparable to the latest developments of new transistors by Intel, which are planned to be ready for production in 2007 [54]. A possibility to form ultrashallow junctions was also shown by using $(SiB_n)^-$ and $(GeB)^-$ cluster ions [55]. Recently, it was found that shallow doping of n- and p-Si by a Ag_n^+ cluster ion beam (implantation energy up to 1 keV) leads to a local modification of

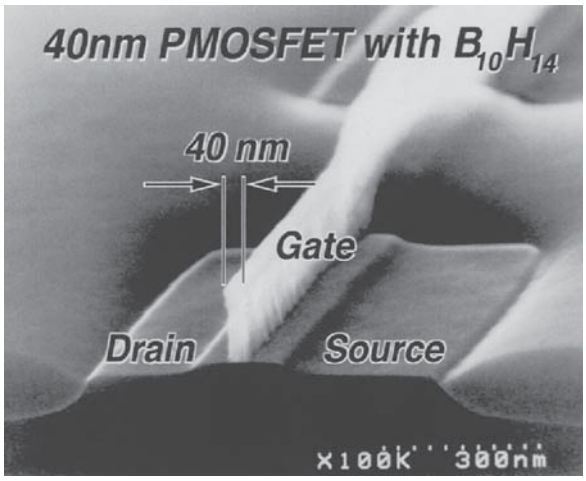

Fig. 4. Cross-sectional SEM image of a p-MOSFET fabricated using implantation of $B_{10}H_{14}$ clusters. Reprinted with permission from [13]. Copyright 2004, Elsevier.

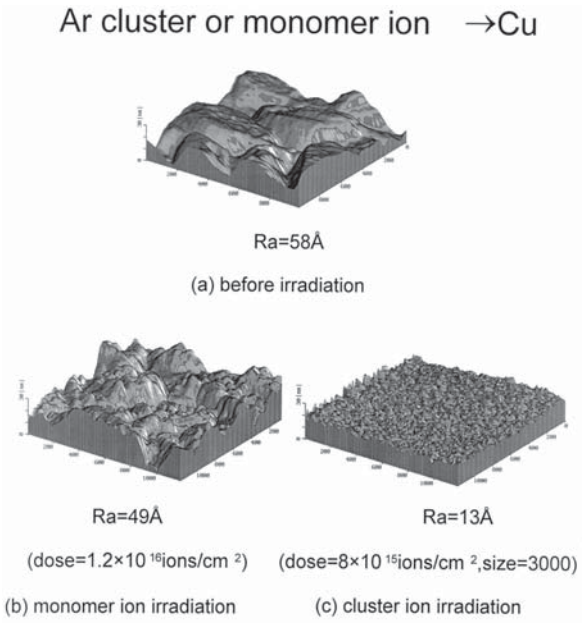

Fig. 5. AFM images of Cu deposited on a Si substrate before and after sputtering by argon monomer and cluster ions. Lateral scales are 1 μm, vertical scale is 30 nm. Reprinted with permission from [13]. Copyright 2004, Elsevier.

the semiconductor energy bands allowing control of the effective Schottky barrier height [56].

In the early 90's, the potential of accelerated large inert gas clusters was explored for surface sputtering and smoothing [12]. Recently, a commercially available technique using gas cluster ion beams (GCIB) has been developed for this purpose [57]. In general, a better smoothing effect was achieved with clusters compared to monomers (see Fig. 5) [53]. The main advantages of cluster use in comparison with ion or plasma assisted processing are also high spatial resolution, short-range damage and elimination of charge accumulation on the substrate surface. Experiments on the angular distribution of material sputtered by diverse cluster ions at different incidence angles and energies have allowed the optimisation of the GCIB technology for surface smoothing, cleaning and etching [58-60]. A better smoothing effect was achieved at low deviation from normal angles of incidence. Increasing the incidence angle of the cluster beam leads to enhanced lateral sputtering of the substrate material (more details about lateral sputtering can be found in section 4). It is important that cluster smoothing does not have a negative effect on the surface mechanical properties. For instance, a TiN surface smoothed by an Ar_n^+ cluster beam did not exhibit any change in its mechanical properties, e.g. nanohardness or residual stress [61].

Dissociation of clusters due to energetic impact can promote chemical reactions on the substrate surface leading to the formation of volatile species and assisting the reactive sputtering of the target. The etching of Si, SiO_2, and W by $(SF_6)_n^+$ cluster ions has been demonstrated [62]. A high sputtering rate allows for very high-speed processing of the surfaces. For instance, for Si substrates bombarded with 45 keV $(SF_6)_n^+$ cluster ions, the sputtering yield reached 2300 atoms/ion that is about 1000 times higher compared to the sputtering by Ar monomer ions [63]. A very high sputtering yield also allows the processing of patterns that are difficult to prepare with traditional plasma etching. Pyrex glass microstructuring by $(CO_2)_n^+$ clusters has shown high efficiency in the formation of regular repeated structures using masks in the beam path to the target [64]. Recently, the applicability of Ar_n^+ cluster ion beams as primary ion beams for secondary ion mass spectrometry has been demonstrated [65]. It was suggested that the effect of local surface sputtering, or crater formation, on cluster-surface impact could be used for hardness measurements. The material hardness can be extracted from the measured crater size if other parameters are known such as the cluster acceleration energy, the sput-

tering yield and the binding energy of the sputtered material [66].

3. CLUSTER BEAM FORMATION

3.1. Generation of clusters

Progress in cluster science has followed closely on the development of experimental techniques. In all cluster sources, cluster generation consists of the following stages: vaporisation (production of atoms or molecules in the gas phase); nucleation (initial condensation of atoms or molecules to form a cluster nucleus); growth (the addition of more atoms or molecules to the nucleus) and coalescence (the merging of small clusters to form larger ones) followed by evaporation (loss of one or more atoms) [1,67,68]. The probability of spontaneous cluster formation under equilibrium conditions is extremely low. Hence, cluster production requires a thermodynamic non-equilibrium that can be implemented by means of a few different types of cluster sources, which are briefly described below.

If the local thermal energy or temperature of the gas consisting of the monomer species is less than the binding energy of the dimer, then a three-atom collision can lead to stable dimer formation. Three atoms are necessary for the fulfilment of energy and momentum conservation:

$$A + A + A \rightarrow A + A_2, \qquad (1)$$

where the third atom (A on the right hand side of the equation) removes the excess energy. To make the nucleation step more efficient, an inert carrier (cooling) gas is often injected into the nucleation chamber of a cluster source. Once the dimer is formed it acts as a condensation nucleus for further cluster growth. Early growth occurs by incorporation of atoms (or molecules) one at a time. Subsequently, collisions between smaller clusters can lead to coalescence and the formation of larger clusters.

In the cluster growth region, the clusters are generally hot, because their growth is an exothermic process, i.e. the internal energy increases due to the heat of condensation of the added atoms. Since the clusters are hot, there is a competition between growth and decay. For practical reasons, i.e. formation of a stable cluster beam, it is often necessary to lower the temperature of the clusters. A few mechanisms can be realised.

Cooling under adiabatic expansion. This mechanism works simultaneously with the cluster formation in the case of supersonic nozzle sources (see next section). A gas under high stagnation pressure is expanded into a vacuum chamber through a nozzle: an abrupt decrease of pressure leads to a drastic temperature decrease in the beam causing supersaturation and, finally, cluster formation [14,69,70].

Collisional cooling. Collisions with other atoms in the beam remove the excess energy from the clusters as kinetic energy:

$$A_n(E_1) + B(\varepsilon_1) \rightarrow A_n(E_2 < E_1) + B(\varepsilon_2 > \varepsilon_1) \qquad (2)$$

where B may be a single atom of element A constituting the cluster or, which is more common, an inert cold carrier gas. E is the internal energy of the cluster species and ε is the kinetic energy of atom B. This cooling mechanism is only significant in the initial expansion and condensation regions.

Evaporative cooling. Clusters can lower their internal energy by evaporation, losing one or more atoms in an endothermal desorption process. The internal energy is channelled statistically into the appropriate cluster vibration mode, in order to overcome the activation barrier for bond breaking. After evaporation, excess energy is imparted as kinetic energy to the escaping atom and daughter cluster:

$$A_n(E_1) \rightarrow A_{n-1}(E_2 < E_1) + A(\varepsilon_1) \rightarrow A_{n-2}(E_3 < E_2) + A(\varepsilon_2) \rightarrow \ldots \qquad (3)$$

This mechanism is the main cooling mechanism once free flight of the cluster has been achieved and there are no collisions.

Radiative cooling. Clusters can also lower their internal energy by emitting radiation:

$$A_n(E_1) \rightarrow A_n(E_2 < E_1) + h\nu \qquad (4)$$

However, radiative cooling is an inefficient cooling mechanism, which is slow compared to the time scale of typical cluster experiments (μs). Electron emission can be an additional channel for cluster cooling especially for fullerenes and some other strongly bonded clusters.

It should be obvious from the discussion above that the clusters are produced in a range of sizes. This size (or mass) distribution can be influenced by the method with which the precursor gas vapour is generated and depends on a number of factors: the initial pressure and temperature; the presence of carrier gas and its parameters; the vacuum conditions and, of course, the variety of technical parameters characterising the cluster source, especially the expansion conditions.

3.2. Cluster sources

Surveys of methods for cluster formation may be found in a number of publications, see for example

[1,67-71]. Here we just briefly introduce the most common approaches used for cluster sources: gas aggregation, supersonic jet, and surface erosion (sputtering).

Effusive and gas aggregation sources. The simplest way to produce small clusters is using a Knudsen cell or effusive source, which is based on the principle of thermal vaporisation of liquids or solids in an oven. Since the vapour is kept in equilibrium in the oven, it is dominated by atoms but there is typically a small fraction of very small clusters (a few atoms in size). The beam of atoms and clusters is formed by effusion through the nozzle into a low-pressure region. The cluster intensity falls exponentially with increasing cluster nuclearity. Hence, this is a low flux continuous subsonic source.

The gas aggregation method is a logical development of the effusive source to enlarge clusters and increase flux intensity. A liquid or solid is evaporated into a carrier gas (He or Ar) cooling the evaporated atoms or molecules and inducing condensation [72]. Once the temperature of the vapour is low enough a stabilising three body collision described by (1) can occur. A smoking fire or cloud and fog formation in nature are good examples of gas aggregation, therefore, this type of source is also called a 'smoking source'. After the aggregation, the clusters expand through the nozzle into the next vacuum chamber forming a subsonic beam. Gas-aggregation cluster sources produce continuous beams of elements with not very high boiling points (< 2000K), usually metals. The cluster size distribution depends on the physical dimensions of the cluster cell and can reach up to a few tens of thousands of atoms in size [73,74]. This type of source is useful for the controllable deposition of size-selected metal clusters and nanostructured thin film growth [75].

Supersonic (free-jet expansion) nozzle sources. These sources exploit the principle of adiabatic expansion of a gas into vacuum. Supersonic nozzle sources are of two types. The sources for cluster generation from gaseous precursors typically operate without a carrier gas. The precursor gas for cluster formation is supplied under high stagnation pressure (from a few up to a few tens of bar) in the pre-expansion reservoir. Seeded supersonic nozzle sources are used to form cluster beams of relatively low-melting-point metals (or liquids), which are vaporised, and the vapour is seeded in the carrier gas at a stagnation pressure of several bars. In both cases either the pure gas or the metal/carrier gas mixture is then expanded through a small-diameter nozzle into vacuum, thereby creating a supersonic cluster beam. More details on the free-jet expansion phenomenon can be found elsewhere [76-78]. Three main factors govern the cluster formation: the stagnation pressure; the temperature and the nozzle characteristics [70,71]. These sources produce intense continuous or pulsed cluster beams with narrow velocity distributions and clusters typically ranging from tens to thousands of atoms depending on the source parameters. Recently, a new gas cluster source with a possibility to get very large Ar clusters (up to 160000 atoms) has been developed [79].

The *surface erosion sources* utilise the removal of atoms and clusters from a solid or liquid surface by laser ablation, arc discharge or heavy ion sputtering.

Laser vaporisation source. The laser vaporisation source is pulsed and used to produce clusters of metals and semiconductors, usually those with high melting points that can not be evaporated by simple heating. In this source, the vapour is produced by the pulsed-laser ablation of the material [80]. Typically, light from a pulsed Nd:YAG or excimer laser is focused on the rod which is driven in a slow screw motion so that a fresh area of its surface continues to be exposed to the laser. Laser ablation can be easily combined with gas aggregation [81]. The vaporised material (plume of plasma with temperature of around 10^4K) is entrained in a pulse of the carrier gas, thus cooling the vapour and causing cluster formation. The gas/cluster mixture is ejected out of the nozzle forming a beam. The use of a laser for cluster generation also leads to some cluster ionisation, so this source generates neutral and charged clusters. The cluster size distribution depends on the source conditions and typically ranges up to few hundred atoms per cluster [82]. One of the advantages of the laser vaporisation source that it is an easy way to produce binary clusters (consisting of two different chemical elements) using binary alloy targets of desired composition [83,84] or a dual-rod configuration [85] or even a dual-rod dual-laser technique [86].

Arc cluster ion source. A source operating on a similar principle as a laser vaporisation source is a pulsed-arc cluster ion source (PACIS) [87], where a rod of material is vaporised by an intense electrical discharge. Typically, about 10% of the emitted material is charged. In general, the cluster beams produced by PACIS tend to be more intensive compared to the laser vaporisation source. Recently, by improvement of source parameters, a cluster deposition rate of about 5 nm/min has been reported [88].

Ion sputtering source. In ion sputtering sources, the cluster ions are produced by bombarding a surface with heavy ions. Ion sputtering sources can be

used to produce clusters of a wide range of materials, especially those with high melting points. In contrast to the previously discussed sources, the sputtering source does not rely on condensation in an inert gas. For cluster production, typically 10-20 keV ion beams of either heavy gases (Kr or Xe) [89,90] or Cs are used. Relatively small (tens of atoms) positively and negatively charged clusters are formed using inert gas sputtering. For the caesium ion sputtering source, predominantly negatively charged clusters are formed, which is related to a minimisation of the work function of the sputtered material by the influence of Cs [91,92]. Typical cluster sizes range from a few up to 20-30 atoms depending on the cluster species [93,94].

Magnetron sputtering source is a modified type of the ion sputtering source where a plasma is ignited in argon over a target surface by applying d.c. or r.f. potentials. The formed clusters can vary in size between 50 and over 10^6 atoms (when combined with a carrier gas); from 20 to 80% of them (depending on cluster species) are ionised [24,95]. Similar to the ion sputtering source, the magnetron source is applicable to a large range of materials. It can provide a cluster beam flux of up to 10^{12} cluster/scm^2 [24]. Recently, a hybrid magnetron sputtering/condensation source combined with a novel time-of-flight mass filter was developed providing intense cluster beams with a constant mass resolution over a broad range of cluster sizes (from 2 to 70000 atoms) [96].

A few more types of cluster sources exist. *Spray sources* are used for generating clusters from liquids and solutions. There are two approaches to make cluster beams: elecrtrospray and thermospray sources. The *electrospray ionisation source* generates solvated ion clusters by the injection of a solution through a needle, which can carry a positive or negative potential, into a stagnation chamber with a flowing inert gas. This method allows complex involatile molecules to be obtained in the gas phase as solvated ions. Electrospray ionisation was introduced in the 60's [97] but it was only in the 90's when it was used for the production of cluster ions, for instance, alkali metal chloride and sodium salt clusters (see references in [98]) or water-methanol, water-glycerol and pure glycerol clusters [99]. In the case of the *thermospray source*, the liquid sample is partly pyrolysed before expansion and a subsonic beam containing neutral and charged clusters is generated. A similar operating principle to the electrospray source can be used for a *liquid-metal ion source*, which is primarily used to produce singly or multiply charged clusters of low-melting-point metals [100-102]. A fine needle under potential is wetted with the metal heated above its melting point. A high electric field at the tip of the needle causes a spray of very small droplets to be emitted. The initially very hot and often multiply ionised droplets undergo evaporative cooling and fission to smaller sizes.

3.3. Ionisation and mass selection of clusters

In many cluster experiments and applications, there is a necessity to mass (size) separate the clusters. For practical reasons, this requires cluster ionisation so that the mass selection can be accomplished by either deflecting the cluster ions in an electromagnetic field or by the time-of-flight (TOF) method. Depending on the cluster species or the object of the experiment, either cations or anions may be created [1].

Positively charged clusters are used more often. There are a few methods to generate cations. One of them is *electron impact ionisation*. This method uses either thermal electrons or a focused accelerated electron beam interacting with the cluster beams. The next possibility is *photoionisation* where laser or other intense light beams (e.g. synchrotron radiation) are used for cluster excitation: photon frequencies can be tuned across a wide range providing a high yield of ionisation with low cluster fragmentation. Positively charged clusters can also be generated by *electric discharge*. This method is used only for free jet sources where a corona discharge occurs within the stagnation chamber, prior to the expansion. To generate anionic clusters, *electron transfer* can be employed. This approach is mainly used in the case of noble metal clusters, which have a relatively high ionisation potential. Electron attachment occurs via collisions with alkali metal atoms in the vapour phase. The disadvantage of this ionisation method is the possibility of alkali metal inclusion into the clusters.

A range of mass separation techniques are available for the charged clusters. Most commonly used are mass spectrometers such as Wien filter, quadrupole, and TOF. Exhaustive reviews on these and some other mass-selecting techniques can be found in [1,5,68,69,71]. The typical mass resolution $\Delta m/m$ of the most common mass spectrometers lies within the range 10^{-4}-10^{-2}. This makes it possible to select the size with a precision of 1 atom for small and medium size clusters.

From the above-presented sections one can see that in the last two decades there has been a growing research interest and activity in various applications of cluster beams as well as in the related technical area of cluster beam production. However, there are still a lot of fundamental physical aspects that have to be studied to provide successful material modification using cluster beams.

4. ENERGETIC DEPOSITION AND IMPLANTATION OF ATOMIC CLUSTERS

Specific phenomena related to cluster-surface impact allow one to divide the use of cluster beams into two categories: *low-energy deposition* and *energetic interaction regimes* (Fig. 6). There is no precise dividing line on the energy scale for those two cases. However, one can consider a process as low-energy when the energy per atom of the accelerated cluster is below the binding energy of the cluster constituents. This case is often called soft landing. The deposition does not induce cluster fragmentation i.e. the clusters preserve their composition. However, the structure can be distorted. This energy regime is normally used to grow porous films and produce special surface relief by cluster assembling. The main problem of soft landing, in terms of some practical applications, is the high surface diffusive mobility of the deposited clusters, leading to either the growth of larger particles (by fusion of small clusters) or cluster coalescence (without fusion) into islands. For more details concerning the soft-landing case one can look elsewhere [4,5,103-105].

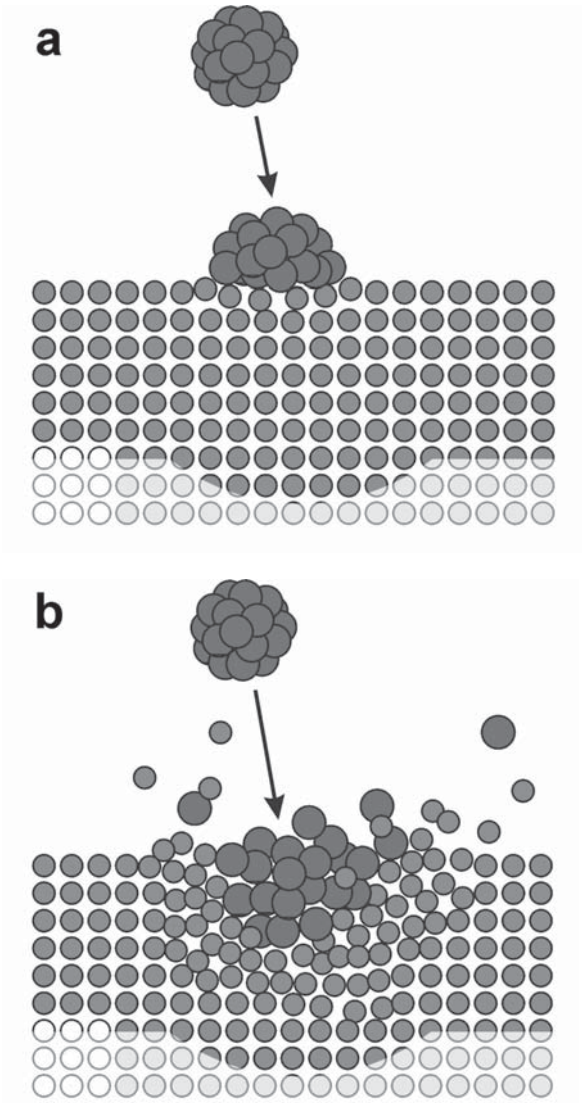

Fig. 6. Schematic pictures of (a) cluster low-energy deposition and (b) energetic impact.

In this paper we mainly discuss the energetic regime, i.e. when the energy per constituent atom given to the cluster by the acceleration (hereinafter cluster energy) is greater than the binding energy of the cluster constituents.

Under energetic impact the cluster loses its structure. The higher the cluster energy, the more the cluster is deformed on surface impact. However, the cluster constituents penetrate into the substrate only if their energy is higher than the penetration threshold energy. Before reaching this value the cluster either breaks up and scatters or flattens on impact. For instance, for Mo_{1043} clusters deposited on a Mo (001) surface, molecular dynamics (MD) simulations showed that clusters with an energy of 1 eV/atom grew a quite dense (up to 80% of the bulk) epitaxial film in which cluster and substrate atoms are mixed just within a distance of one lattice constant [10]. Further increase of the cluster energy up to 10 eV/atom led to the complete decomposition of the clusters and formation of a denser film with better adhesion to the substrate because of the strong intermixing between cluster and substrate material within a few atomic layers. The formation of the thin dense films was favoured by the high density of energy deposited by the clusters. Despite the quite low energy per atom, multiplication of this relatively low energy by the number of atoms and division by the very small surface collision area leads to high values of the energy density. It was also simulated that the energetic cluster deposition suppresses the surface roughness of

the deposited film because of a new smoothing mechanism due to a so-called 'downhill particle current' transporting hills of the film into valleys [106]. Hence, the predicted energetic regime of about 10 eV/atom for metal clusters is most appropriate for thin film growth by energetic cluster deposition. This was experimentally demonstrated by deposition of very smooth (roughness of 0.7-1.5 nm), dense and strongly adhering coatings on Si, quartz and steel substrates using Al_n^+, $(TiN)_n^+$ and $(TiAlN)_n^+$ cluster ions with energies of 5-20 eV/atom [11].

One of the interesting boundary cases (between soft landing and implantation) is so-called pinning when the energetic cluster disrupts the substrate lattice, such that a few atoms from the surface layer are displaced and some of the cluster atoms implant [107]. The pinning process suppresses the cluster diffusion on the surface. It was experimentally found, for example, for the case of Ag_n^+ cluster ions (n=50-200) implanted into graphite that the pinning threshold energy is about 10 eV/atom [41]. Good agreement between the experiments and MD simulations for this case was achieved (Fig. 7). The pinned clusters create binding sites that can be used for immobilisation of sequentially deposited objects, for instance, organic molecules [42,108].

It should be noted that the obtained pinning threshold energy for silver clusters impacting graphite is in agreement with the above-mentioned cluster energy leading to the decomposition of molybdenum clusters and their intermixing with the surface layer of the substrate. Hence, in both cases atoms of the clusters are able to penetrate into the substrate matrix with an energy as low as ca. 10 eV/atom. This value is significantly lower than penetration threshold energies for any monomer ions implanted into different target materials. For example, it is known that for graphite the penetration threshold increases with the ion radii and the minimum value was found to be 22.5 eV for light He^+ ions [109]. This is, therefore, one of the clear cases where cluster-surface impact is different from monomer ion impact.

Due to the large size and weak bonding between atoms, cluster implantation is fundamentally different from that of monomer ion implantation [110]. Clusters generate multiple-collision effects during the penetration into the target. The effect of the high

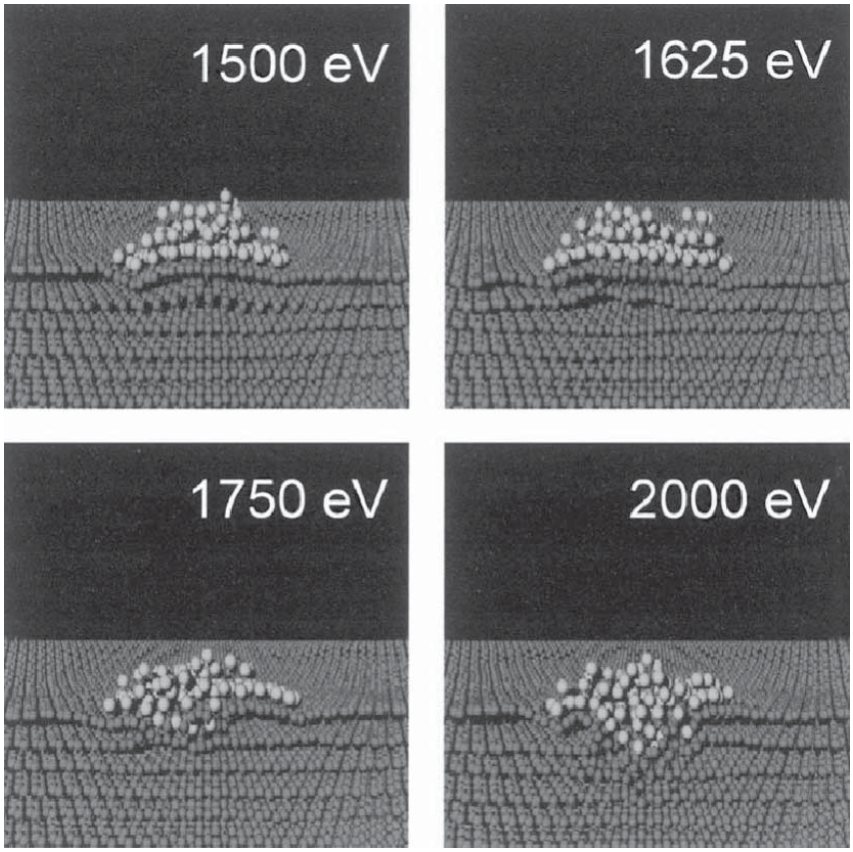

Fig. 7. MD simulations, viewed in cross section, of the impact of Ag_{147} cluster at various energies (indicated in the panels) with graphite. Reprinted with permission from [41]. Copyright 2000, American Institute of Physics.

density of the energy transferred from cluster to the target at the beginning of impact can be compared with a microexplosion or to some extent with a nanoscopic analogue of a meteorite-planet collision that typically results in crater formation [111]. One more peculiarity of the cluster-solid interaction is nonlinearity, which arises from the fact that the cluster atoms influence each other during the penetration into the target and thus the environment in the material is different for each atom or ion of the cluster. Nowadays there is no commonly-accepted theory satisfactorily describing the cluster implantation process. However, below we present some critical analysis of the published data on the subject.

It was shown by MD simulations of implantation of various cluster species that the clusters break down into single atoms quite rapidly under impact: after some tens or hundreds of femtoseconds depending on the cluster size, energy and target material [112-114]. For slow cluster constituents (from tens of eV to tens of keV per atom) the energy loss occurs predominantly due to elastic collisions between the atoms. Hence, one can expect an overlapping of the collision cascades originating from the individual cluster atoms during their penetration into the target. Thus, the difference between the stopping of an atom in a cluster and an individual atom makes a difference to the projected range R_p of cluster constituents and hence to the produced radiation damage compared to monomer ion implantation. MD and Monte Carlo simulations showed that the penetration depth of clusters is larger than for the corresponding ions at the same incident velocity [115-117]. It was suggested that a so-called 'clearing-the-way effect', where the 'front' atoms of the cluster push target atoms out of the way, could take place. Heavier ions would thus be expected to cause more clearing of 'light' targets [118]. On the contrary, the effect is negligible if the mass of the cluster constituents is much smaller than the mass of the target atoms, as was shown, for instance, for the simulations of deuterium cluster implantation (clusters of up to 500 atoms with energy of 200 eV/atom) into a silver target [119]. As a result of the 'clearing-the-way' the stopping power of the cluster is reduced and the projected range is increased.

Up to now, the simulations showed different scaling laws for diverse implantation conditions. For instance, in the case of Ar_n (n = 43 and 688) cluster implantation into silicon with energies E between 10 and 100 eV/atom it is calculated that $R_p \sim E^{1/3}$ and the penetration depth depends rather on the total cluster energy than on the cluster size (for n from 43 to 688) [112]. However, for smaller clusters, Ar_6 and Ar_{13}, the effect of size on R_p was found to be more significant and the R_p values were comparable to those of monomers if the energy per cluster atom was the same as the monomer ion energy. Contrary to this simulation, modelling of implantation of small Au_n (n = 2-7) clusters into Cu with energies of 1-10 keV/atom showed an increase of R_p with the cluster size for the same energy per cluster atom [114]. Calculations of implantation of Si_n clusters ($n \leq 50$) into Si with a constant energy of 70 eV/atom also confirmed the dependence of R_p on the cluster size, the penetration depth scaled approximately as $n^{1/3}$ [120]. The dependence of R_p on the implantation energy (up to 70 eV/atom) for Si_{50} gave the scaling law~ $E^{1/2}$, which is different from the above-mentioned $E^{1/3}$ predicted for the Ar_n clusters. This discrepancy can be related to the difference in the 'clearing-the-way' effect for different cluster species. Simulations of Au_n (n = 1,13,43,87,201,402) cluster implantation into gold and graphite targets with an energy of 100 eV/atom showed a clear effect of the cluster size on the ranges and the dependence followed a power law $R_p = an^{\alpha}$ with α varying from 0.31 to 0.45, when changing from gold to graphite [121]. The value of α obtained for the gold target is in agreement with the value for the implantation of Si_n clusters into Si. The difference in α for the gold clusters implanted into graphite is easily explained in term of more 'clearing' for targets composed of 'light' atoms.

The 'clearing-the-way' effect was experimentally found in the case of small Ta_n^+ clusters (n=2,4,9) implanted into graphite with an energy of 555 eV/atom, however no scaling dependence was suggested [122]. Experiments on the implantation of polyatomic (up to 4) boron ions into silicon also showed an increase in both the projected range and straggling in the case of clusters compared to monomers for about 20 and 30%, respectively [123]. For C_{60}^+ ion implantation into graphite within a rather wide range of energies from 500 eV to 23 keV the penetration depth was found to follow $E^{1/2}$ [124]. The clearing-the-way effect was also demonstrated for graphite bombarded by positively- and negatively-charged Ag_n clusters. However, the estimated implantation ranges were found to scale proportionally to the cluster momentum [125,126].

Cluster ranges were also found to be effected by the high density of energy deposited by the cluster due to thermal spikes [127,128]. In the case of keV-energy cluster implantation the spike originates via nuclear stopping of the projectiles, i.e. by energy deposited in ion-atom and atom-atom collisions

during the ballistic (or dynamic) phase of the collision cascades. The impacted area experiences both high temperature and pressure transients. Local temperature and pressure can rise up to 10^4-10^5K and the GPa level, respectively, for the first 10^{-13} - 10^{-12} s [129-131] that leads to local melting around the ion tracks. Interestingly, the temperature and pressure values are comparable to those obtained for meteorite-planet impacts [132]. Violent interaction under the cluster impact leads to local melting of the target material. The calculated effective radius of the molten regions, for example, in Cu was about 2 nm per cascade [133]. MD simulations showed an increase in the range straggling ΔR_p (up to 130%) of Au_n clusters implanted into Cu with energies of 1-10 keV/atom compared to monomers due to atomic mixing in the thermal spike [114]. However, this theory predicts that no increase in the ΔR_p of cluster constituents is expected for Si because the cascades break down into subcascades at much lower energies compared to Cu and the liquid-like pockets are much smaller and cool down faster. Similar to this simulation, there was no difference in the R_p and a very small difference in the ΔR_p found when comparing the calculated values for B_1 and B_{10} implanted into Si with energies of 200 and 500 eV/atom [134]. The theoretically predicted change (or its absence) in R_p and ΔR_p is in good correlation with the experimentally obtained depth profiles of Au_n^+ (n = 2, 3, 7) cluster ions implanted into copper and silicon with energies of 10-100 keV/atom [135].

Thus, so far MD simulations and experiments do not yet allow the formulation of a universal law for cluster projectiles and their stopping in matter. This problem can be related to both the approaches used in the simulations and the experimental methods employed to obtain the projected ranges. In particular, empirical potentials used for MD were originally constructed and tested for crystal lattices near thermodynamic equilibrium and it is not a surprise that applied to collision simulations the quantitative results are not in complete agreement. In the case of experiments with keV-energy clusters the errors in the determination of R_p can be rather high due to very shallow implantation, especially for the case of graphite where the R_p is measured as the depth of etched pits [125,126]. This corresponds more to the depth of the radiation damage than to the projected range.

Despite the statement that the nuclear stopping should dominate for clusters from the first atomic layer of the substrate, it was found that electronic stopping becomes important due to an effect originated from the fact that the cluster constituents may interact in a coherent way with the medium. This is called the vicinage effect. The electron vicinage effect leads to enhancement of the cluster stopping power (energy loss) compared to monomers as a result of interference in the excitation of target electrons by the simultaneous interactions with a few ions (cluster constituents or recoils). This phenomenon was experimentally observed for the first time on implantation of swift proton diatomic and three-atomic cluster ions into carbon and gold [20] and a little later it was explained theoretically [136,137]. However, this effect is found to be important mainly for very high implantation energies (MeV-GeV range) [138].

During the last decade, there has been increasing interest in implantation of MeV clusters showing specific phenomena like giant track and hillock (nm-size surface protrusion) formation in various target materials [139-141]. The observed radiation damage is confined inside 20-40 nm diameter cylinders around the projectile paths and related to the strong localisation of the deposited energy via electronic stopping, in particular due to the collective electronic excitation [142]. Only particles with high-energy loss and low velocity, which correspond more to the case of clusters than to monomers, are found to produce tracks yielding significant hillock formation [143]. Recently, the state-of-the-art of high-energy cluster implantation has been summarised and analysed in [144]. A ‘compound spike’ model including thermal and ion explosion spikes dominating at certain stages of the track formation is proposed. For the stopping power, contributions from each ion as well as from vicinage effects between the ions and from additional plasma stopping were suggested to be taken into account. The possibility of a dense highly ionised transient plasma in the initial stage of cluster penetration followed from the vicinage effect, i.e. from the interaction between close spatially correlated ions in the field of the free target electrons produced on a time scale comparable to the time ~ d/v, where d is mean distance between the ions and v is their velocity [145].

A closely-related problem to the estimation of the cluster stopping and projected range is the radiation damage in the target. Unfortunately, this question has been poorly experimentally studied for the keV-energy range so far. MD simulations of Ar_n clusters impacting on Si showed that a similar damage region is formed by both large (hundreds of atoms) and small (tens of atoms) clusters if the total implantation energy (energy per cluster) is the same (Fig. 8) [112]. In other words, an increase in cluster

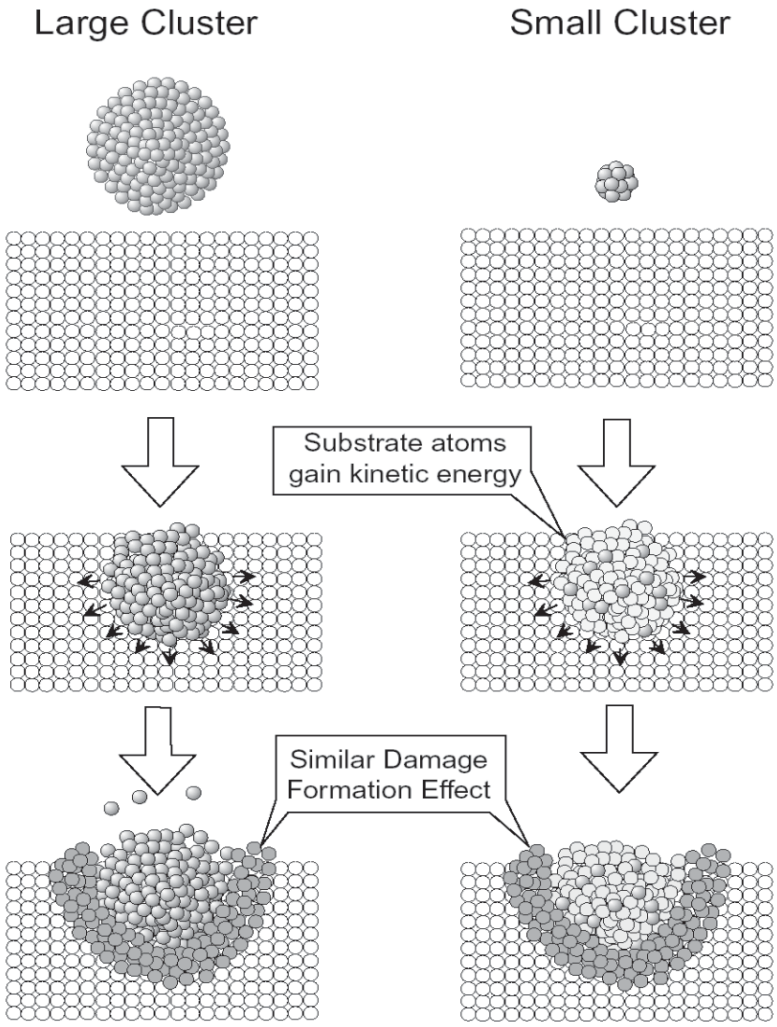

Fig. 8. Model of damage formation by impact of large and small clusters. Reprinted with permission of T. Aoki from [112].

size leads to a decrease in the threshold energy of damage formation and to an increase of the displacement yield [146]. The latter is confirmed by other simulations. Simulations of Ta_n cluster implantation into graphite evidenced a superlinear increase in the number of damages (vacancies) with cluster size at the same energy per cluster atom [147]. In the simulations of B_4 and B_{10} clusters implanted into Si with an energy of 230 eV/atom it was found that the clusters produced a several times larger number of Frenkel defects (vacancies and interstitials) compared to B monomers [148]. The damaged region was also found to be characterised by a high yield of amorphisation especially for the larger cluster B_{10}. Experiments on boron dimers and trimers implanted into Si with an energy of 1 keV/atom qualitatively confirmed the simulations by demonstrating that the number of displaced silicon atoms per cluster atom increased by a factor of a two compared to the monomer implantation [149].

A very high sputtering yield induced by cluster bombardment has been theoretically predicted and experimentally observed on various types of surfaces [12,58-61,150,151]. The sputtering is caused by the violent impact, semi-spherical shock wave and crater formation. As a result of high-energy transfer to the target the atomic arrangement in the crater region becomes highly disordered. These atoms possess high kinetic energy and a large fraction of them – those present in the crater rim – obtain momenta

directed away from the surface. The MD simulations of the sputtering yield Y from various metal surfaces by Ar_n cluster bombardment with keV energies fit a power law dependence $Y \sim E^{1.4}$, where E is the total cluster energy [152]. This dependence is found to be in reasonable agreement with experimental results on Ar_n^+ cluster beam sputtering of various metal surfaces [153]. The obtained power exponent 1.4 is close to the value 1.5 found in a thermal spike model of supersonic velocity impact of macroscopic particles [154]. In the experiments on Si sputtering by keV Au_n^+ cluster bombardment, it was found that Y slightly increases with cluster size without a significant change in the number of produced surface defects [150]. High values of Y for clusters compared to monomers were explained as being due to so-called lateral sputtering effects originated by a shock wave. At normal impact angle of the cluster beam, the angular distribution of the sputtered target atoms has a non-symmetric shape, which is different from the 'cosine' distribution caused by monomers (Fig. 9) [12,13]. In the case of sputtering, the cluster energy should be high enough to provide displacements of the target atoms but not too high to avoid implantation and radiation damage of the substrate. The high sputtering yield and relatively low radiation damage of the target by large keV clusters are two important features allowing efficient surface cleaning using inert gas cluster ion beams [53].

The specific dynamics of the sputtering on cluster impact also leads to the possibility of using cluster beams for surface smoothing as mentioned in section 2 of this review. According to MD simulations, the driving force for the smoothing mechanism can be thought of as a high non-equilibrium surface diffusivity of target atoms in the rim of the crater [59]. The rough surface can be modelled as a sequence of hills and valleys. The simulations showed that if the cluster hits the central part of a hill the material is efficiently removed. A valley impact leads to much lower sputtering yield. When the cluster impacts a slope a downhill particle current transferring the material into the valley is induced [59,155]. Thus, the height difference between hills and valleys is decreased and the surface becomes smoother. It was shown that the smoothing effect could be increased by use of higher impact energies and smaller clusters [155]. However, too small clusters with higher energies can penetrate more deeply causing significant radiation damage. Therefore, in practice there should always be a compromise between the cluster size and impact energy.

Additionally to the above-discussed 'physical sputtering', a mechanism of so-called 'chemical sputtering' or reactive accelerated cluster erosion (RACE) was suggested [64]. In experiments on 120 keV $(CO_2)_n^+$ cluster impact with diamond and copper substrates, despite the predicted much higher erosion rate (about 2 orders of magnitude) of copper compared to diamond the experimentally found rates were of the same order of magnitude. It was assumed that the very high temperatures reached on the hypervelocity cluster impact lead to the dis-

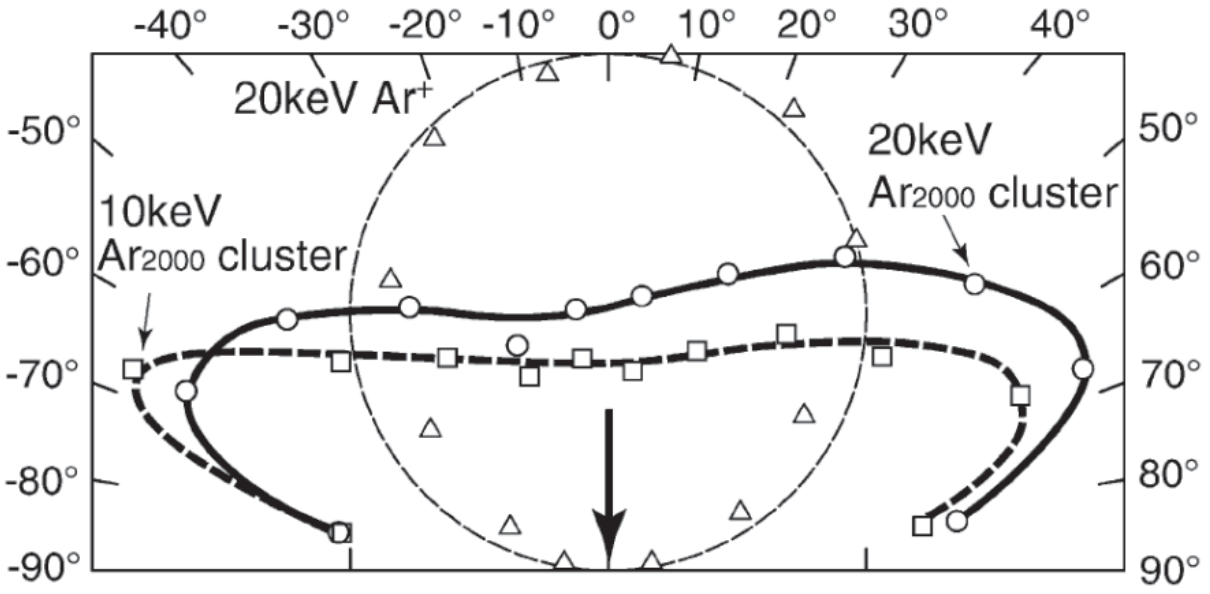

Fig. 9. Angular distribution of Cu atoms sputtered by Ar monomer and cluster ions at normal incidence. Reprinted with permission from [13]. Copyright 2004, Elsevier.

sociation of the CO_2 molecules and the resulting atomic oxygen reacted with the target material. In the case of copper a low-vapour-pressure oxide was formed while for the diamond a highly volatile CO compound was the resulting product. The 'chemical sputtering' mechanism was later confirmed by experiments with $(SF_6)_n^+$ cluster ions bombarded into W, Au, Si, and SiC [156]. For example, in the case of 20 keV cluster ions comprised of 2000 SF_6 molecules, each constituent has an energy of 10 eV which is lower than the displacement energy of Si (about 15 eV), i.e. lower than the threshold energy for physical sputtering. However, the sputtering yield of Si by $(SF_6)_{2000}^+$ cluster ions was found to be 55 times higher than by Ar_{3000}^+ cluster ions. The sputtering yield was also found to increase exponentially with the cluster energy. The high yield of volatile SF_x compounds was registered by a residual gas analyser confirming the chemical nature of the sputtering. The effect of lateral sputtering for the 'chemical case' is eliminated which is caused by the isotropic evaporation of volatile materials produced by the chemical reactions. By mask protective patterning of the surfaces, i.e. by selective etching, RACE was suggested as a cluster impact lithography method for obtaining specific surface micron or submicron relief (Fig. 10) [13].

Cluster impact chemistry is one more chemical case to use energetic cluster beams [157,158]. Molecular clusters impacting a solid surface with hypersonic velocities (1-10 km/s) are the ideal approach to explore chemical and physical processes at extraordinarily high pressures and temperatures on a nanometre scale. Moreover, clusters can be regarded as a perfectly defined reaction system with a freely adjustable composition of the reactants. From a chemical point of view, the energy range from 0.1 eV/molecule to about 10 eV/molecule is especially interesting, as it allows fragmentation of the cluster, dissociation of the molecules within the cluster, and formation of new chemical bonds without destroying the solid substrate. Thus, not only dissociation of chemical bonds can occur within a cluster compressed by the impact on a solid surface but also bond formation is possible in the very short time between cluster impact and subsequent cluster fragmentation [159]. The variation in collision energy then allows a change in the rate of the excitation of cluster vibrations, the total internal energy content, and the particle density. Recently, the effects of cluster dissociation and intercluster reactions on impact as well as electronic interaction between clusters and surfaces were comprehensively reviewed in [160].

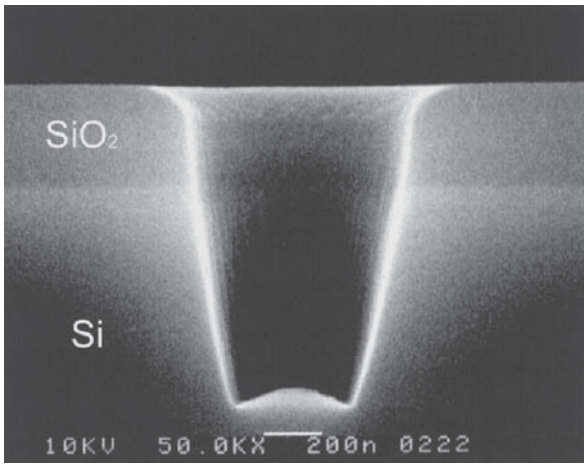

Fig. 10. SEM image of Si/SiO_2 substrate etched by $(SF_6)_n^+$ cluster ions with an energy of 20 keV. Reprinted with permission from [13]. Copyright 2004, Elsevier.

Energetic cluster-surface impact results in an atomic pair interaction within the cluster due to collisions between the 'front layer' of the atoms that already met the surface and the incoming rest of the cluster constituents. According to MD simulations, this interaction can result in outer-shell electronic excitation, multiple ionisation and inner-shell Auger excitation of the cluster constituents [161,162]. However, it is a challenging task to resolve experimentally the electron emission originated by the compressed cluster atoms from that due to the emission from the surface atoms [163]. The latter is caused by the excitation of the target electrons on the high-energy transfer from the cluster to a local substrate area at the impact spot on a time scale of 10^{-14}-10^{-13} s [164]. The electron emission from the surface was found to be dependent on the surface composition and its cleanness: in general, 'dirtier' surfaces yield more emission; the relative yield is higher from metals than from semiconductors or dielectrics [163]. It was also found that negatively charged clusters give a higher electron emission yield than positively charged ones [164]. The emission under cluster impact exhibits a so-called sublinear effect that manifests in a decrease of the electron yield per cluster atom with an increasing number of atoms in the cluster [164,165]. Recently, a 'sweeping-out-electrons' effect was suggested to explain the decrease in the electron emission by removing some electrons from the cluster path by the front running cluster atoms [166]. This phenom-

enon is similar to the 'clearing-of-the-way' effect but for the electronic system of the target.

5. CRATER FORMATION ON ENERGETIC CLUSTER IMPACT

Considerable attention has been given to the erosion of surfaces under the impact of energetic particles. One of the first observations of crater formation on a target surface after heavy-ion sputtering was published at the beginning of the 80's [167]. A transmission electron microscopy (TEM) study of Bi^+ and Bi_2^+ ion implanted Au surfaces showed the existence of small craters with a mean diameter of about 4-5 nm. It was found that the number of craters per incident ion is rather low and increases from $< 10^{-3}$ to 10^{-2} in the range of 50-125 keV implantation energy. In the case of diatomic molecules, the increase in density of impact energy because of simultaneous overlapping of two cascades caused a reduction in the threshold energy for crater formation and strongly increased crater yields. Later, craters were found on impact of various keV ions with different materials by scanning probe microscopy [168-171]. In contrast to the first observation, there was a 1:1 correlation between the craters observed and the areal density of ion impacts for implantation energies up to 200 keV [168,171]. For the case of Kr^+, As^+, and Ge^+ ions implanted into PbS and Si, the crater diameter was found to be an increasing function of the energy until it reached 200 keV [168]. The diameters varied from 7 to 28 nm. With further energy increase the crater diameter and the crater/impact ratio decreased: craters were not found for implantation energies as high as 1 MeV. In the case of the first crater observations the modified thermal-spike model, introduced by Seitz and Koehler [172] and developed by Kelly [127], was used to explain the crater formation associated with individual displacement cascades originated by the penetrating particles. Wilson *et al.* suggested a more detailed description in which they assumed that the centre of the cascade is rich in vacancies and the periphery in interstitials. This causes stresses leading to compaction or sinking of the central part and peripheral rising forming the crater rims [168].

By both MD simulations [124,130,173-176] and experiments [58,131,177], it was shown that energetic cluster-surface impact causes crater formation. The crater can be surrounded by a few E high rim formed by the substrate material displaced from the central part of the crater to its edges as shown, for example, for the case of C_{60}^+ impact on graphite with energies of 1.85-4.0 keV [177]. The physics of the crater formation is quite well understood and the simulations agree well with the experimental data. The crater diameter was found to be an increasing function of both the cluster size and energy [66]. For instance, in the case of Ar clusters consisting of a few hundred up to a few thousand atoms and energies between 20-150 keV the crater diameters on Si and Au surfaces were measured to be from 4 to 35 nm [66,131,178]. However, the crater formation rate decreases with increase of energy per cluster constituent [179]. This is probably related to an increase of the projected range and,

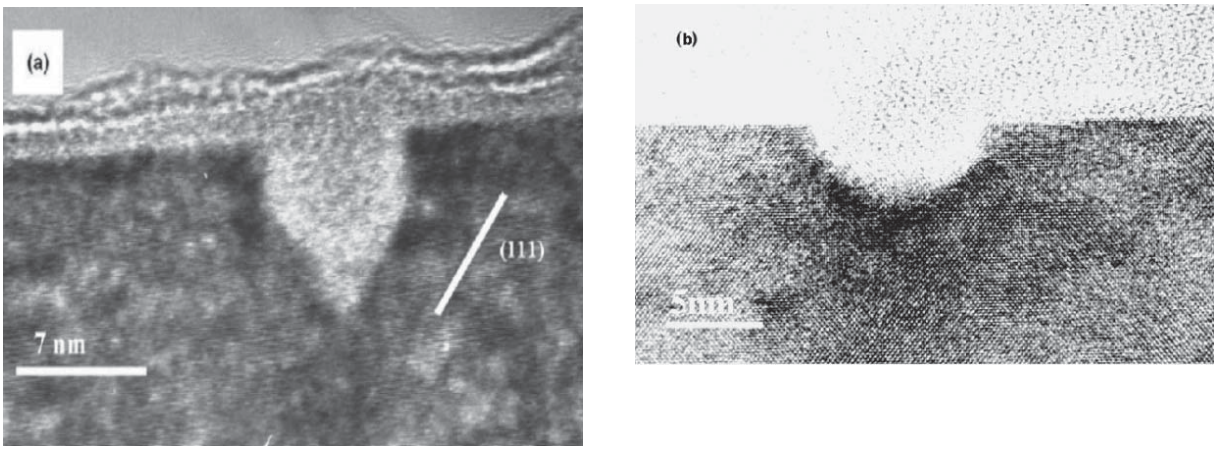

Fig. 11. TEM cross-sectional images of (a) individual 24 keV Ar_n^+ cluster ion impact on Si(100) and (b) individual 24 keV $(O_2)_n^+$ cluster ion impact on Si(111). Reprinted with permission from [180]. Copyright 2003, Elsevier.

as a result, to a shift of the maximum of the cluster-to-substrate energy transfer into the sample. Thus, the tendencies for crater formation (diameter and rate) as the implantation energy is increased are in qualitative agreement with those mentioned above for monomer ion implantation. Using high resolution TEM, cross-sectional images of the craters were obtained showing a dependence of the crater shape on the crystallographic orientation of the target material: near conical with the facet directed along the (111) plane for Si(100) and hemispherical for Si(111) (Fig. 11) [131,180].

Recently, along with craters, hillocks (nm-size protrusions) were found experimentally on keV-energy cluster impact [131,181-183]. The hillock dimensions and their shape depend on cluster species, substrate material and implantation conditions. One of the first observations was obtained on Si impacted by $(CO_2)_n^+$ clusters with an average size of 1000 molecules and energy of 100 keV/cluster [181]. In this case the hillock height was only about 0.5 nm as found by atomic force microscopy (AFM). Cone-shaped hillocks with a height of a few nm and basal diameter of about 20-40 nm were found by AFM on HOPG, Si and metal surfaces implanted by $(CO_2)_n^+$ cluster ions with a mean size of 750 molecules and energies of 40-60 keV [182]. Similar hillocks were observed on Si and ITO surfaces bombarded by nitrogen, oxygen and argon clusters (from 20 to 100 atoms in size) with energies of 3-15 keV (Fig. 12) [183]. On Si impact by 24 keV large Ar_n^+ (n =1000-10000) clusters, the hillocks observed by AFM varied in height up to 4 nm and had a basal

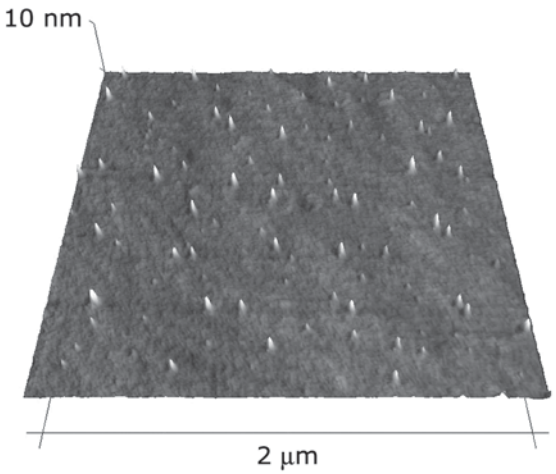

Fig. 12. AFM image of a Si surface implanted by 3 keV Ar_{12}^+ cluster ions.

diameter of ~40 nm. However, their shape was not simply cone-like. Typically, distinct dimples were found at the tops of the hillocks. Similar to the craters (see above), these tops (rim surrounding the dimples) showed a dependence in shape on Si crystal symmetry: three-fold symmetry was observed for the top part of the hillocks on Si(111) while four-fold symmetry for those on Si(100) (Fig. 13) [131,180].

Despite a few orders of magnitude difference in energy, the hillocks formed on implantation of clusters with MeV-GeV energies into various metal, semiconductor and dielectric targets have a similar height (a few nm) and basal diameter (20-40 nm)

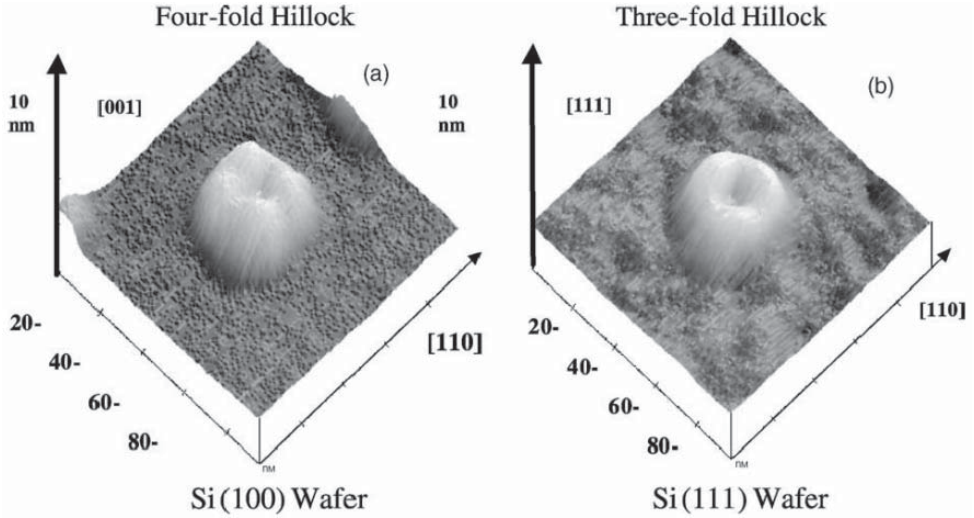

Fig. 13. AFM images of hillocks formed by 24 keV Ar_n^+ cluster ion impact on (a) Si(100) and (b) Si(111). Reprinted with permission from [180]. Copyright 2003, Elsevier.

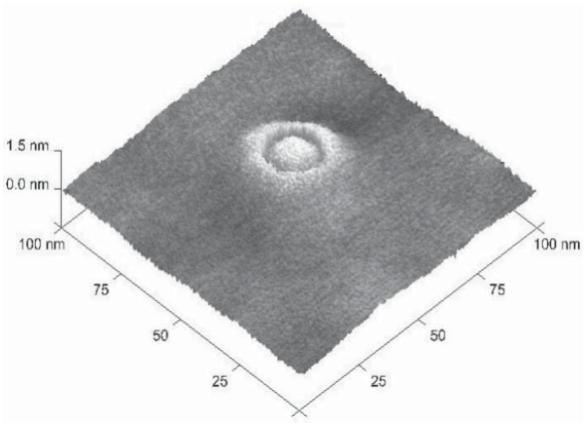

Fig. 14. Complex crater with a diameter of 18 nm on a Si surface implanted by 18 keV Ar_{12}^{+} cluster ions.

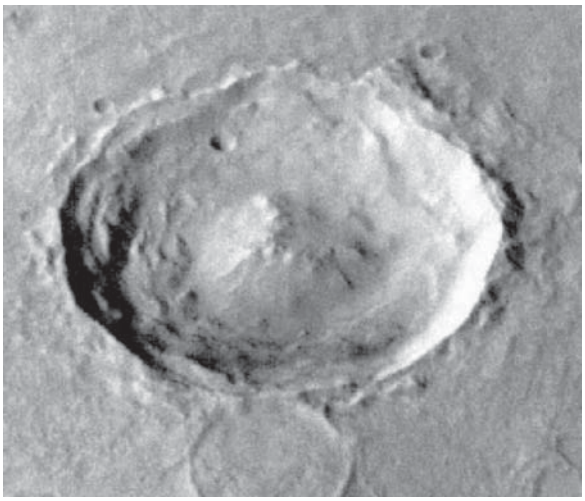

Fig. 15. Yuty crater on Mars with a diameter of 18 km as imaged by the Viking Orbiter (free download from <www.lpi.usra.edu>).

[141-143,184,185]. There are also a number of publications on hillock formation by swift heavy ions, for instance [186-189]. Recently, it was shown that the hillocks formed on irradiation of $Fe_{0.55}Zr_{0.45}$ alloy by MeV C_{60}^{+} ions [184] have a centrally located dimple similar to those found on Si under keV-energy impact of large Ar clusters. Several models were applied to explain the hillock formation on high-energy implantation. Among the most important are the shock wave, Coulomb explosion, ionic and thermal spikes or 'compound spike' mentioned above [143,144,185,189]. Despite minor discords of the existing approaches, the mechanism of hillock formation under MeV-energy bombardment can be ascribed as a result of electronic stopping in the wake of the cluster or their constituents leading to local melting along the track, pushing out and quenching the molten material. However, for low-energy (tens keV) cluster implantation, the origins of hillock formation are only beginning to be studied.

In recent experiments on both monomer ion and cluster ion implantation with keV energies it was found that a cone-shaped hillock can be located in the centre of the crater (i.e. surrounded by a rim) forming a so-called complex crater (Fig. 14), by analogy with those made by meteorite impact on a planet surface (Fig. 15) [190,191]. Until this observation, complex crater structures were found only for swift heavy ion irradiation of sapphire [187]. In the case of Si implanted by 1.5 keV Ar^{+} and N^{+} ions the number of the simple and complex craters was found to be comparable [191]. It could be that in the case of simple craters the hillocks were too small to be detected on the bottom of the craters by AFM due to the finite size of the tip used. Some of the simple craters were reminiscent of the hillocks in shape, i.e. were truncated cones with a dimple at the top. The hillock basal diameter and the simple crater diameter were found to be of the same value, about 10-15 nm. The wall to wall diameter of the rims in the complex craters was between 20-40 nm. The rim height was about 0.5 nm. The height of the hillocks varied from 0.5 to 2.0 nm. An increase of implantation energy led to the gradual disappearance of the hillocks. For monomer ion implantation with an energy of 6 keV they are no longer found. Simulations using the SRIM-2003 code [192] showed that for 1.5 keV Ar^{+} ions about 78% and 22% of the total ion energy is lost due to nuclear and electronic stopping, respectively. In the case of such a low-energy implantation there is not significant difference in the depth profiles of energy loss for those two stopping mechanisms. The ion stopping leads to an effective heat transfer to the matrix within the first few nanometers of the range. Hence, one can assume that the hillocks are a result of a local surface thermal effect causing shallow-layer melting at the collision spot with subsequent liquid melt out and quenching.

Numerous MD simulations of keV-energy monomer and cluster impact on solids predicted very high

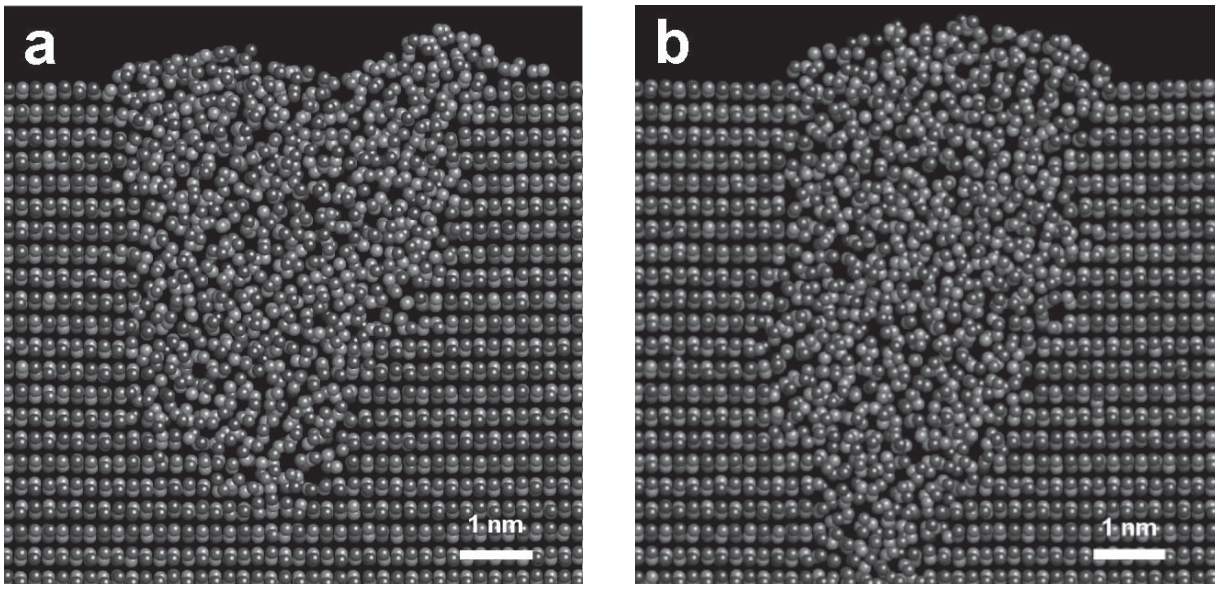

Fig. 16. Snapshots of MD simulations of 15 keV Ar_{12} cluster implantation into Si (20 ps after the impact) [196].

local temperatures and pressures (about 10^4K and 10^{10} Pa) resulting in melting of the material surrounding the tracks [129-131]. It was observed in the simulations of monomer impact that a hot melt can be forced onto the surface by the thermal expansion or pressure in the cascades [193,194]. This viscous flow can form a small bump (below 1 nm in height) at the impact spot. Despite these predictions, up to now the MD simulations of cluster impacts using Stillinger-Weber, Tersoff, ZBL potentials or their combination, which fit quite well to silicon, diamond or metal substrates, showed only crater formation with just a limited possibility of a small peak in the crater [195]. Only recently, simulations of 15 keV Ne_{12} and Ar_{12} clusters implanted into Si(111) using a modified Tersoff III potential with an extended range of interaction between the Si atoms compared to the standard Tersoff III showed a possibility of both crater (Fig. 16a) and hillock (Fig. 16b) formation [196]. However, the hillock basal diameter and height were still found to be much smaller compared to those experimentally observed (see below). Hence, the nature of a significant expulsion effect leading to a few nm high hillocks is an open question for further investigations.

Since the complex crater formation provides a nanoscopic analogue of meteorite-planet collisions and there are developed models of the complex crater formation on meteorite impact one could try some of those approximations [197] for the cluster impact modelling. The use of the formula for a hypervelocity impact based on Euler's equations and presented in [198] allows a numerical calculation of the volume of melted material V_m:

$$\frac{V_m}{R_{pr}^3} \propto f(\rho_{pr},\rho_t)\left(\frac{E_m}{\nu^2}\right)^{-\frac{3\mu}{2}}, \qquad (5)$$

where R_{pr} is the projectile radius, ρ_{pr} and r_t are projectile and target densities, respectively, E_m is the specific heat of target melting, ν is the projectile velocity and the parameter μ varies between 1/3 and 2/3 depending on whether the melt scaled with the momentum or with the energy of the impactor.

In the case of an Ar cluster, R_{pr} and ρ_{pr} were calculated by assuming an icosahedral packing of Ar atoms with Van der Waals radii, ρ_t and E_m were taken to be the parameters for bulk silicon [190]. Varying m showed unreasonably small and large V_m values for the boundary conditions, i.e. for μ =1/3 (momentum scaled) and μ = 2/3 (energy scaled), respectively. The meteorite-impact simulations showed that μ is equal to 0.58 for metals and 0.47 for porous solids [198]. The use of $\mu \approx 0.50$-0.55, which is an intermediate value between those two, for example, for simulation of the 3 keV Ar_{12}^+ cluster impact with Si gave a melted volume from 92 to 246 nm^3. The hillock volume obtained from the AFM measurements varied from 84 to 196 nm^3 (a conical

shape was assumed for determining the volume). This was considered as a reasonable agreement taking into account that not all molten material forms the hillock and the hillock could also contain a cavity. However, it was found that with respect to prediction of the hillock size Eq. (5) can be adopted only for a limited number of cases, presumably, for very low implantation energies and small clusters. The problem is that Eq. (5) predicts the molten volume but not the expulsion effect. According to the equation, the molten volume should increase with the impact energy but experimentally with an increase in energy and cluster size a decrease in hillock volume was observed [191,199]. This effect on the hillock formation will be discussed below.

Thus, unfortunately, up to now modelling of keV-energy cluster impact does not provide realistic physical origins for the hillock formation. Below, a qualitative picture of the hillock appearance based on systematic experimental studies of cluster ion implantation is discussed showing tendencies in the hillock formation depending on cluster species, size and energy as well as on type of substrate.

Simple and complex craters similar in dimensions to those mentioned above for the Ar^+ and N^+ ion implantation into Si were recently found on 3-18 keV Ar_n^+ and Xe_n^+ cluster ion implantation into silicon and sapphire [190,191,199]. The following mechanism was proposed for the complex crater formation: an impacting cluster ion generates multiple collision cascades overlapping with each other in a very narrow surface region of the solid material. The kinetic energy of the cluster constituents is transferred to the substrate atoms mainly via the nuclear stopping mechanism (low-energy cluster implantation). Other effects such as shock-waves as well as efficient ionisation in the material also play an important role in the evolution of defects during the very first picoseconds following the impact. A high density of energy deposition results in a local melting of a shallow layer of the material around the impact spot. Because of the difference in densities of the hot fluidised material and the surrounding crystalline material as well as due to elastic rebound of the bulk or local tensions, the liquid melt is pushed away (expulsed) from the surface. The subsequent rapid quenching of the melted material results in the formation of a hillock which is surrounded by the rim of the crater wall. Due to significant material intermixing in the collision spot there is a probability for some of the cluster atoms to remain in the target during its re-solidification. Therefore, one can expect that the hillock interior contains cluster atoms alongside small cavities, as indicated by recent MD simulations [196].

When comparing the results of Ar_n^+ cluster ion implantation into two different materials, silicon and sapphire, under the same conditions the following tendencies for crater and hillock formation were found: 1) complex craters appear at higher implantation energies on sapphire than on silicon; 2) for implantation of light clusters (Ar_{12}^+) the hillocks are higher on silicon than on sapphire until the hillocks become comparable in height with the surrounding rims at implantation energies of 15 and 18 keV/cluster; 3) there is, in general, a higher rate of simple craters compared to complex craters for sapphire than for silicon (Fig. 17).

In terms of radiation damage and energy transfer from an impacting projectile to the material, sapphire has higher displacement energy (for both Al and O atoms) as well as higher melting point compared to Si. Therefore, at identical implantation conditions argon cluster ions should produce a smaller melted volume in sapphire than in silicon. In agreement with this, the hillocks resulting from the melt quenching were more pronounced on the silicon compared to sapphire (Fig. 18). For the same reason the energy window for hillock formation on sapphire was shifted towards higher implantation energies and there were many more simple craters found on sapphire than on silicon. In general, vanishing of the hillocks at high implantation energies for any type of substrate indicates the surface nature of hillock formation, i.e. that the cluster-to-target energy transfer processes are shifted deeper into the bulk. This observation is in agreement with the empirical dependence of the cluster implantation range as a linear function of the cluster momentum [125,126].

A difference in impact dynamics of various cluster ion species was stressed earlier. One of the examples is from a comparison of $Ar_n^+$and Xe_n^+ cluster implantation into silicon [199]. For the Xe-implanted silicon, the same tendency in crater formation as for the Ar-implanted one was found. At the lowest implantation energy of 3 keV/cluster mostly complex craters were formed. However, the rate for formation of simple craters gradually increased with the implantation energy and this type of defect dominated for heavier clusters (Ar_{54}^+ and Xe_{16}^+). The mean diameters of the simple and complex craters, ca. 10-20 and 20-40 nm respectively, measured using AFM, were found to be very similar for both species. The energy window for hillock formation in both cases is also quite similar. However, the hillocks produced by the Xe_4^+ clusters were found to be lower than those formed by the Ar_{12}^+ clusters. The data on

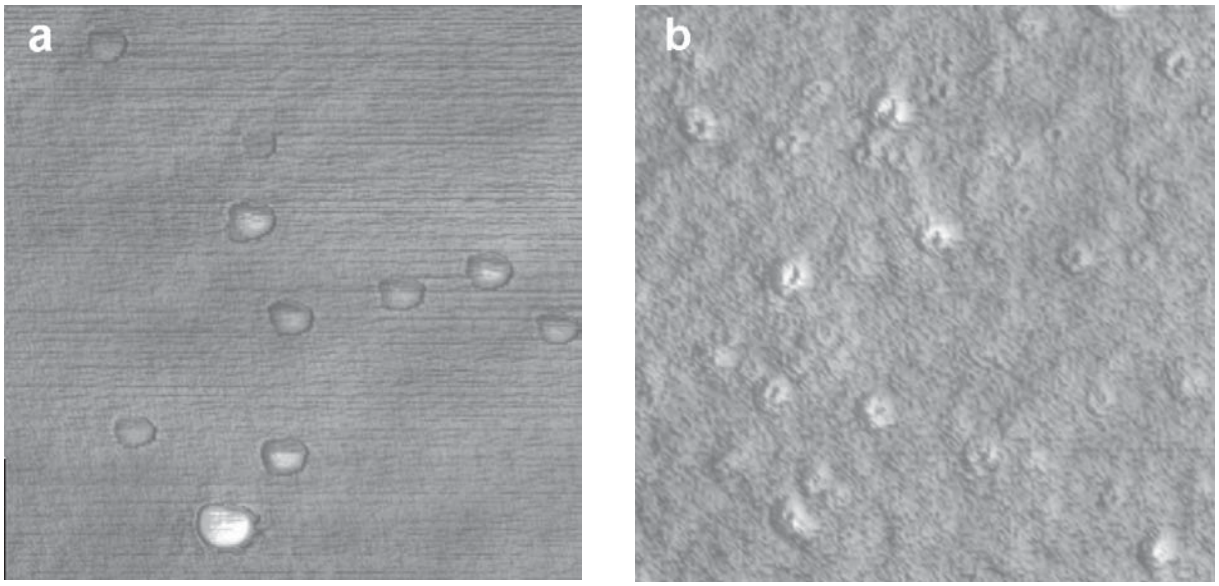

Fig. 17. AFM images (500×500 nm) of (a) silicon and (b) sapphire surfaces implanted by 6 keV Ar_{12}^{+} cluster ions.

hillock height are presented in Fig. 19. While analysing the impact of Ar_n^+ and Xe_n^+ clusters with close total mass and the same implantation energy, one can expect higher projected ranges for the xenon constituents due to the higher momentum per cluster atom. Hence, the cluster-to-target energy transfer due to stopping of Xe is shifted slightly deeper into the substrate, which can lead to a decrease of the surface melting. As mentioned in [195], upon cluster break up, atoms of heavier elements damp the motion of target atoms more efficiently than those of lighter ones. Thus, smaller hillocks from Xe_n^+ cluster ion bombardment can be explained (i) by slightly higher projected ranges of the xenon cluster constituents decreasing the surface melting and (ii) by a suppression in the expulsion effect due to the damping of the motion of silicon atoms by the heavier xenon atoms.

Summarising the discussion about the hillock formation on keV-energy cluster implantation one can emphasise the following: (i) the hillocks are formed as a result of local surface melting caused by the energy transfer from the cluster constituents; (ii) the origins of the significant expulsion effect are not well understood but could be related to the difference in densities of the hot fluidised material and the surrounding solid state matrix as well as to elastic rebound of the bulk or local tensions in the substrate; (iii) the size of the hillocks is a decreasing function of both the cluster size and energy, the vanishing of the hillocks with increase of implantation energy is probably related to the shift of the cluster-to-target energy transfer deeper into the substrate; (iv) the size of the hillocks depends on the cluster species, if the cluster atoms are heavier than the substrate ones the expulsion effect is sup-

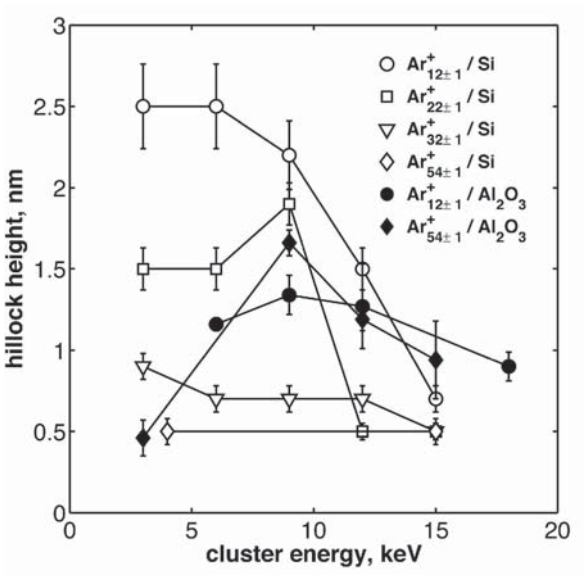

Fig. 18. Hillock height on silicon and sapphire vs implantation energy of Ar_n^+ cluster ions.

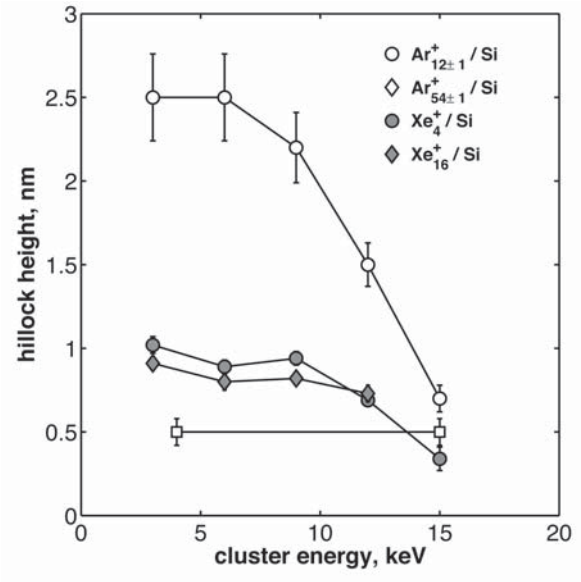

Fig. 19. Hillok height on silicon vs implantation energy of Ar^+_n and Xe^+_n cluster ions.

pressed due to the damping of the motion of light substrate atoms by heavy cluster atoms; (v) the characteristics of the substrate material play an important role, hillocks are more pronounced for substrates with a low displacement energy and melting point.

6. CONCLUSIONS

The field of cluster physics is about 50 years old. Despite this age, quite a lot of questions related to cluster formation and cluster properties are still under discussion and this is of great importance for understanding the fundamental physics of the transitional form of matter in the growth from single atom to bulk.

At the same time, there is a new intensively developing area utilising the cluster beams for modification of material properties, synthesis of nanostructures and a variety of applications in material science, electronics and optics. Summarising the data presented in this review on practical applications, one can conclude that the energetic cluster deposition technique has a number of advantages compared to other methods for synthesis of very thin and atomically smooth films. These films can be used as insulating layers and protecting or wear-resistant coatings for submicron and nanodevices [44-46,48,49]. Formation of nanostructured films and deposition of selective clusters of noble metals are promising directions for optics where either plasmon resonance phenomenon or luminescent properties of the nanostructures can be utilised [27, 34-36]. Non-linear optical characteristics of such systems are also under investigation. Thus, cluster beams can be considered as an alternative approach for the developing plasmonics and nanophotonics research areas. Use of clusters of transition metals (Fe, Co, Ni, *etc.*) imbedded into dielectric matrices is studied for fabrication of magneto-sensitive and memory devices [8,9,37-40]. The possibility to immobilise organic molecules on clusters pinned to surfaces opens a way to biological and medical applications [42]. Shallow cluster implantation is a method of significant importance for modification of properties of thin surface layers in electronics [12,55,56]. The high yield of sputtering by cluster beams is already commercially utilised for surface cleaning and etching of materials [57].

Despite the wide area of cluster applications, the physics of energetic cluster interaction with surfaces and cluster stopping in solids is poorly understood so far. There are new phenomena such as, for example, 'clearing-the-way', 'compound spike', 'chemical etching', complex crater formation that have recently been found on cluster impact or implantation. These effects explain some particular cases of the energetic cluster-solid interaction. However, there are a number of contradictory reports of the different experiments and disagreements between some experiments and theory. At present, theoretical simulations and experiments do not allow the formulation of a universal law for stopping of cluster projectiles in matter. It is to be hoped that the increasing amount of systematic experimental data will lead to an improvement in the situation in the near future.

REFERENCES

[1] R.L. Johnston, *Atomic and Molecular Clusters* (Taylor&Francis, London, 2002).
[2] T.P. Martin // *Phys. Rep*. **273** (1996) 199.
[3] L. Bardotti, B. Prevel, P. Jensen, M. Treilleux, P. Melinon, A. Perez, J. Gierak, G. Faini and D. Mailly // *Appl. Surf. Sci.* **191** (2002) 205.
[4] A. Perez, P. Melinon, V. Dupius, P. Jensen, B. Prevel, J. Tuaillon, L. Bardotti, C. Marlet, M. Treilleux, M. Broyer, M. Pellarin, J.L. Vaille, B. Palpant and J. Lerme // *J. Phys. D: Appl. Phys.* **30** (1997) 709.
[5] C. Binns // *Surf. Sci. Rep.* **44** (2001) 1.

[6] W. Harbich, S. Fedrigo and J. Buttet // *Chem. Phys. Lett*. **195** (1992) 613.
[7] U. Kreibig and M. Vollmer, *Optical Properties of Metal Clusters* (Springer, Berlin, 1995).
[8] D.L. Peng, K. Sumiyama, T. Hihara, S. Yamamuro and T.J. Konno // *Phys. Rev. B* **61** (2000) 3103.
[9] A.L. Stepanov, R.I. Khaibullin, B.Z. Rameev, A. Reinholdt, R. Pecenka and U. Kreibig, In: *Nanostructured Magnetic Materials and Their Applications*, ed. by B. Aktas, L. Tagirov and F. Mikailov (Kluwer, Dordrecht, 2004) p. 23.
[10] H. Haberland, Z. Insepov and M. Moseler // *Phys. Rev. B* **51** (1995) 11061.
[11] Y. Qiang, Y. Thurner, Th. Reiners, O. Rattunde and H. Haberland // *Surf. Coat. Technol.* **100-101** (1998) 27.
[12] I. Yamada and J. Matsuo // *Mat. Res. Soc. Symp. Proc.* **427** (1996) 265.
[13] I. Yamada, J. Matsuo, N. Toyoda and A. Kirkpatrick // *Mater. Sci. Enging R* **34** (2001) 231.
[14] E.W. Becker, K. Bier and W. Henkes // *Z. Phys*. **146** (1956) 333.
[15] W. Henkes *// Z. Naturforschg*. **16a** (1961) 842.
[16] W. Henkes // *Z. Naturforschg*. **17a** (1962) 786.
[17] J. Bauchert and O.-F. Hagena // *Z. Naturforschg*. **20a** (1965) 1135.
[18] H. Burghoff and J. Gspann // *Z. Naturforschg*. **22a** (1967) 684.
[19] E.W. Becker, R. Klingelhöfer and H. Mayer // *Z. Naturforschg*. **23a** (1968) 274.
[20] W. Brandt, A. Ratkowski and R.H. Ritchie // *Phys. Rev. Lett*. **33** (1974) 1325.
[21] T. Takagi, I. Yamada and A. Sasaki // *Thin Sol. Films* **39** (1976) 207.
[22] I. Yamada and T. Takagi // *Thin Sol. Films* **80** (1981) 105.
[23] I. Yamada, H. Takaota, H. Usui and T. Takagi // *J. Vac. Sci. Techn. A* **4** (1986) 722.
[24] H. Haberland, M. Karrais, M. Mall and Y. Thurner // *J. Vac. Sci. Techn. A* **10** (1992) 3266.
[25] H. Haberland, Z. Insepov, M. Karrais, M. Mall, M. Moseler and Y. Thurner // *Mat. Sci. Eng. B* **19** (1993) 31.
[26] J.L. Xu, J.L. Chen and J.Y. Feng // *Nucl. Instr. Meth. B* **194** (2002) 297.
[27] M. Ehbrecht, B. Kohn, F. Huisken, M.A. Laguna and V. Paillard // *Phys. Rev. B* **56** (1997) 6958.
[28] P. Milani, M. Ferretti, P. Piseri, C.E. Bottani, A. Ferrari, A. Li Bassi, G. Guizzetti and M. Patrini // *J. Appl. Phys.* **82** (1997) 5793.
[29] E. Barborini, P. Piseri, A. Podesta and P. Milani // *Appl. Phys. Lett.* **77** (2000) 1059.
[30] E. Magnano, M. Padovani, V. Spreafico, M. Sancrotti, A. Podesta, E. Barborini, P. Piseri and P. Milani // *Surf. Sci.* **544** (2003) L709.
[31] L. Ravagnan, F. Siviero, C. Lenardi, P. Piseri, E. Barborini and P. Milani // *Phys. Rev. Lett.* **89** (2002) 285506.
[32] *Carbyne and Carbynoid Structures*, ed. by R.B. Heimann, S.E. Evsykov and L. Kavan (Kluwer, Dordrecht, 1999).
[33] H.-J. Gao, S.J. Pang and Z.Q. Xue, In: *Electrical and Optical Polymer Systems*, edited by D.L. Wise, G.E. Wnek, D.J. Trantolo, T.M. Cooper and J.D. Gresser (Marcel Dekker: New York, 1998), p. 729.
[34] M. Gartz, C. Keutgen, S. Kuenneke and U. Kreibig // *Eur. Phys. J. D* **9** (1999) 127.
[35] B. Palpant, B. Prevel, J. Lerme, E. Cottancin, M. Pellarin, M. Treilleux, A. Perez, J.L. Vialle and M. Broyer // *Phys. Rev. B* **57** (1998) 1963.
[36] A. Khabari, F.K. Urban III, P. Griffiths, I. Petrov, Y.-W. Kim and C. Bungay // *J. Vac. Sci. Technol. B* **21** (2003) 2313.
[37] P. Melinon, V. Paillard, V. Dupius, A. Perez, P. Jensen, A. Hoareau, J.P. Perez, J. Tuaillon, M. Broyer, J.L. Vialle, M. Pellarin, B. Baguenard and J. Lerme // *Int. J. Mod. Phys. B* **9** (1995) 339.
[38] C. Binns, S.H. Baker, M.J. Maher, S. Louch, S.C. Thornton, K.W. Edmonds, S.S. Dhesi and N.B. Brookes // *Phys. Stat. Sol. (a)* **189** (2002) 339.
[39] D.L. Peng, T. Hihara, K. Sumiyama and H. Morikawa // *J. Appl. Phys.* **92** (2002) 3075.
[40] P. Zhang, F. Zuo, F.K. Urban III, A. Khabari, P. Griffiths and A. Hosseini-Tehrani // *J. Mag. Magnet. Mater.* **225** (2001) 337.
[41] S.J. Carroll, S. Pratontep, M. Streun, R.E. Palmer, S. Hobday and R.Smith // *J. Chem. Phys.* **113** (2000) 7723.
[42] R.E. Palmer, S. Pratontep and H.-G. Boyen // *Nature Mater.* **2** (2003) 443.
[43] B. Prevel, L. Bardotti, S. Fanget, A. Hannour, P. Melinon, A. Perez, J. Gierak, G. Faini, E. Bouris and D. Mailly // *Appl. Surf. Sci*. **226** (2004) 173.

[44] J. Matsuo, E. Minami, M. Saito, N. Toyoda, H. Katsumata and I. Yamada // *Eur. Phys. J.: D* **9** (1999) 635.
[45] N. Toyoda, Y. Fujiwara and I. Yamada // *Nucl. Instr. Meth. B* **206** (2003) 875.
[46] O. Nakatsu, J. Matsuo, K. Omoto, T. Seki, G. Takaoka and I. Yamada // *Nucl. Instr. Meth. B* **206** (2003) 866.
[47] H. Yamashita and M. Anpo // *Catal. Surv. Asia* **8** (2004) 35.
[48] X.R. Zou, J.Q. Xie and J.Y. Feng // *Surf. Coat. Technol*. **111** (1999) 119.
[49] A. Akizuki, J. Matsuo, I. Yamada, M. Harada, S. Ogasawara and A. Doi // *Nucl. Instr. Meth. B* **112** (1996) 83.
[50] J.R. Engstrom, D.J. Bonser, M.M. Nelson and T. Engel // *Surf. Sci*. **256** (1991) 317.
[51] A.P. Caricato, m. De Sario, M. Fernandez, G. Leggieri, A. Luches, M. Martino and F. Prudenzano // *Appl. Surf. Sci*. **197-198** (2002) 458.
[52] A. Cremona, L. Laguardia, E. Vassallo, G. Ambrosone, U. Coscia, F. Orsini and G. Poletti // *J. Appl. Phys*. **97** (2005) 023533.
[53] I. Yamada, J. Matsuo, N. Toyoda, T. Aoki, E. Jones and Z. Insepov // *Mater. Sci. Enging. A* **253** (1998) 249.
[54] <www.intel.com/update/contents/si07031.htm>
[55] X. Lu, L. Shao, X. Wang, J. Liu, W.-K. Chu, J. Bennet, L. Larson and P. Ling // *J. Vac. Sci. Technol. B* **20** (2002) 992.
[56] B. Cvikl, D. Korosak and Zs.J. Horvath // *Vacuum* **50** (1998) 385.
[57] A. Kirkpatrick // *Nucl. Instr. Meth. B* **206** (2003) 830.
[58] N. Toyoda, H. Kitani, N. Hagiwara, T. Aoki, J. Matsuo and I. Yamada // *Mater. Chem. Phys.* **54** (1998) 262.
[59] N. Toyoda, N. Hagiwara, J. Matsuo and I. Yamada // *Nucl. Instr. Meth. B* **161-163** (2000) 980.
[60] J.A. Greer, D.B. Fenner, J. Hautala, L.P. Allen, V. DiFilippo, N. Toyoda, I. Yamada, J. Matsuo, E. Minami and H. Katsumata // *Surf. Coat. Technol*. **133-134** (2000) 273.
[61] A.J. Perry, S.J. Bull, A. Dommann, M. Michler, B.P. Wood, D. Rafaja and J.N. Matossian // *Surf. Coat. Technol*. **140** (2001) 99.
[62] I. Yamada // *Nucl. Instr. Meth. B* **148** (1998) 1.
[63] T. Seki and J. Matsuo // *Mat. Res. Soc. Symp. Proc.* **792** (2004) R9.29.
[64] J. Gspann // *Nucl. Instr. Meth. B* **112** (1996) 86.
[65] N. Toyoda, J. Matsuo, T. Aoki, Sh. Chiba, I. Yamada, D.B. Fenner and R. Torti // *Mat. Res. Soc. Symp. Proc.* **647** (2001) O5.1.
[66] Z. Insepov, R. Manory, J. Matsuo and I. Yamada // *Phys. Rev. B* **61** (2000) 8744.
[67] M.M. Kappes and S. Leutwyler, In: *Atomic and Molecular Beam Methods*, Vol. 1, ed. by G. Scoles (Oxford University Press, Oxford, 1988) p. 380.
[68] W.A. de Heer //*Rev. Mod. Phys*. **65** (1993) 611.
[69] H. Haberland, In: *Clusters of Atoms and Molecules*, Vol. 1, ed. by H. Haberland (Springer, Heidelberg, 1994) p. 207.
[70] H. Pauly, *Atom, Molecule, and Cluster Beams*, Vol. 2 (Springer, Berlin, 2000).
[71] P. Milani and S. Iannotta, *Cluster Beam Synthesis of Nanostructured Materials* (Springer, Berlin, 1999).
[72] K. Sattler, J. Mühlbach and E. Recknagel // *Phys. Rev. Lett.* **45** (1980) 821.
[73] T.P. Martin, T. Bergmann, H. Göhlich and T. Lange // *Chem. Phys. Lett.* **172** (1990) 209.
[74] H. Abe, W. Schulze and B. Tesche // *Chem. Phys.* **47** (1980) 95.
[75] I.M. Goldby, B. von Issendorff, L. Kuipers and R.E. Palmer // *Rev. Sci. Instrum.* **68** (1997) 3327.
[76] O.F. Hagena // *Surf. Sci.* **106** (1981) 101.
[77] D.R. Miller, In: *Atomic and Molecular Beam Methods*, Vol. 1, ed. by G. Scoles (Oxford University Press, Oxford, 1988) p.14.
[78] H. Pauly, *Atom, Molecule, and Cluster Beams*, Vol. 1 (Springer, Berlin, 2000).
[79] T. Seki, J. Matsuo, G.H. Takaoka and I. Yamada // *Nucl. Instr. Meth. B* **206** (2003) 902.
[80] T.G. Dietz, M.A. Duncan, D.E. Powers and R.E. Smalley // *J. Chem. Phys.* **74** (1981) 6511.
[81] P. Milani and W.A. de Heer // *Rev. Sci. Instr.* **61** (1990) 1835.
[82] N. Saito, K. Koyama and M. Tanimoto // *Appl. Surf. Sci.* **169-170** (2001) 380.
[83] S. Nonose, Y. Sone, K. Onodera, S. Sudo and K. Kaya // *J. Phys. Chem*. **94** (1990) 2744.
[84] J.L. Rousset, A.M. Cadrot, F.J. Cadete Santos Aires, A. Renouprez, P. Melinon,

A. Perez, M. Pellarin, J.L. Vialle and M. Broyer // *J. Chem. Phys.* **102** (1995) 8574.
[85] R.L. Wagner, W.D. Vann and A.W. Castleman // *Rev. Sci. Instr.* **68** (1997) 3010.
[86] W. Bouwen, P. Thoen, F. Vanhoutte, S. Bouckert, F. Despa, H. Weidele, R.E. Silverans and P. Lievens // *Rev. Sci. Instr.* **71** (2000) 54.
[87] G. Gantenför, H.R. Siekmann, H.O. Lutz and K.-H. Meiwes-Broer // *Chem. Phys. Lett.* **165** (1990) 293.
[88] E. Barborini, P. Piseri and P. Milani // *J. Phys. D: Appl. Phys.* **32** (1999) L105.
[89] P. Fayet, J.P. Wolf and L. Wöste // *Phys. Rev. B* **33** (1986) 6792.
[90] T. Leisner, S. Vajda, S. Wolf and L. Wöste // *J. Chem. Phys.* **111** (1999) 1017.
[91] G.D. Alton // *Nucl. Instr. Meth. A* **244** (1986) 133.
[92] J. Ishikawa // *Rev. Sci. Instr.* **63** (1992) 2368.
[93] S.G. Hall, M.B. Nielsen, A.W. Robinson and R.E. Palmer // *Rev. Sci. Instr.* **68** (1997) 3335.
[94] X.M. Wang, X.M. Lu, L. Shao, J.R. Liu and W.K. Chu // *Nucl. Instr. Meth. B* **196** (2002) 198.
[95] H. Haberland, M. Mall, M. Moseler, Y. Qiang, T. Reiners and Y. Thurner // *J. Vac. Sci. Technol. A* **12** (1994) 2925.
[96] S. Pratontep, S.J. Carroll, C. Xirouchaki, M. Streun and R.E. Palmer // *Rev. Sci. Instr.* **76** (2005) 045103.
[97] M. Dole, L.L. Mack, R.L. Hines, R.C. Mobley, L.D. Ferguson and M.B. Alice // *J. Chem. Phys.* **49** (1968) 2240.
[98] C. Hao, R.E. March, T.R. Croley, J.C. Smith and S.R. Rafferty // *J. Mass Spectrom.* **36** (2001) 79.
[99] J. F. Mahoney, E. S. Parilis and T. D. Lee // *Nucl. Instr. Meth. B* **88** (1994) 154.
[100] A. Dixon, C. Colliex, R. Ohana, P. Sudraud and J. Van de Walle // *Phys. Rev. Lett.* **46** (1981) 865.
[101] H. Helm and R. Möller // *Rev. Sci. Instr.* **54** (1983) 837.
[102] N.D. Bhaskar, C.M. Klimcak and R.P. Frueholz // *Rev. Sci. Instr.* **61** (1990) 366.
[103] P. Jensen // *Rev. Mod. Phys.* **71** (1999) 1695.
[104] W. Harbich, In: *Metal Clusters at Surfaces*, ed: by K.-H. Meiwes-Broer (Springer, Berlin, 2000) p. 107.
[105] K. Seeger and R.E. Palmer, In: *Metal Clusters at Surfaces*, ed. by K.-H. Meiwes-Broer (Springer, Berlin, 2000) p. 275.
[106] M. Moseler, O. Rattunde, J. Nordiek and H. Haberland // *Comput. Mater. Sci.* **10** (1998) 452.
[107] S.J. Carroll, P. Weibel, B. von Issendorff, L. Kuipers and R.E. Palmer // *J. Phys.: Condens. Matter* **8** (1996) L617.
[108] J.A. Collins, C. Xirouchaki, R.E. Palmer, J.K. Heath and C.H. Jones // *Appl. Surf. Sci.* **226** (2004) 197.
[109] D. Marton, H. Bu, K.J. Boyd, S.S. Todorov, A.H. Al-Bayati and J.W. Rabalais // *Surf. Sci. Lett.* **326** (1995) L489.
[110] T. Takagi // *Mater. Sci. Enging. A* **253** (1998) 30.
[111] R.S. Averback and M. Ghally // *Nucl. Instr. Meth. B* **90** (1994) 191.
[112] T. Aoki, *PhD Thesis*, Kyoto University, 2000.
[113] C.F. Sanz-Navarro, R. Smith, D.J. Kenny, S. Pratontep and R.E. Palmer // *Phys. Rev. B* **65** (2002) 165420.
[114] J. Peltola and K. Nordlund // *Phys. Rev. B* **68** (2003) 035419.
[115] Y. Yamamura // *Nucl. Instr. Meth. B* **33** (1988) 493.
[116] Y. Yamamura and T. Muramoto // *Rad. Eff. Def. Sol.* **130-131** (1994) 225.
[117] V.I. Shulga and P. Sigmund // *Nucl. Instr. Meth. B* **47** (1990) 236.
[118] V.I. Shulga, M. Vicanek and P. Sigmund // *Phys. Rev. A* **39** (1989) 3360.
[119] Y. Yamamura and T. Muramoto // *Nucl. Instr. Meth. B* **72** (1992) 331.
[120] G.H. Gilmer, C. Roland, D. Stock, M. Jaraiz and T. Diaz de la Rubia // *Mater. Sci. Enging B* **37** (1996) 1.
[121] C. Anders and H.M. Urbassek // *Nucl. Instr. Meth. B* **228** (2005) 57.
[122] C.T. Reimann, S. Andersson, P. Brühwiler, N. MÍrtensson, L. Olsson, R. Erlandsson, M. Henkel and H.M. Urbassek // *Nucl. Instr. Meth. B* **140** (1998) 159.
[123] J.H. Liang and H.M. Han // *Nucl. Instr. Meth. B* **228** (2005) 250.
[124] R.P. Webb, M. Kerford, M. Kappes and G. Brauchle // *Nucl. Instr. Meth. B* **122** (1997) 318.
[125] S. Pratontep, P. Preece, C. Xirouchaki, R.E. Palmer, C.F. Sanz-Navarro, S.D. Kenny and R. Smith // *Phys. Rev. Lett.* **90** (2003) 055503.

[126] L. Seminara, P. Convers, R. Monot and W. Harbich // *Eur. Phys. J. D* **29** (2004) 49.
[127] R. Kelly // *Rad. Eff.* **32** (1977) 91.
[128] A. Miotello and R. Kelly // *Nucl. Instr. Meth. B* **122** (1997) 458.
[129] Ch.L. Cleveland and U. Landman // *Science* **257** (1992) 355.
[130] T.J. Colla, R. Aderjan, R. Kissel and H.M. Urbassek // *Phys. Rev. B* **62** (2000) 8487.
[131] L.P. Allen, Z. Insepov, D.B. Fenner, C. Santeufemio, W. Brooks, K.S. Jones and I. Yamada // *J. Appl. Phys*. **92** (2002) 3671.
[132] H.J. Melosh, *Impact Cratering: A Geologic Process* (Oxford Univ., New York, 1989).
[133] H. Hsieh, T. Diaz de la Rubia and R.S. Averback // *Phys. Rev. B* **40** (1989) 9986.
[134] Y. Hada // *Physica B* **340-342** (2003) 1036.
[135] H.H. Andersen, A. Johansen, M. Olsen and V. Touboltsev // *Nucl. Instr. Meth. B* **212** (2003) 56.
[136] N.R. Arista and V.H. Ponce // *J. Phys. C* **8** (1975) L188.
[137] N.R. Arista // *Phys. Rev. B* **18** (1978) 1.
[138] N.R. Arista // *Nucl. Instr. Meth. B* **164-165** (2000) 108.
[139] H. Dammak, A. Dunlop and D. Lesueur // *Phys. Rev. Lett.* **74** (1995) 1135.
[140] A. Brunelle, S. Della-Negra, J. Depauw, D. Jacquet, Y. Le Beyec, M. Pautrat and Ch. Schoppmann // *Nucl. Instr. Meth. B* **125** (1997) 207.
[141] P. Thevenard, J.P. Dupin, Vu Thien Binh, S.T. Purcell, V. Semet and D. Guillot // *Nucl. Instr. Meth. B* **166-167** (2000) 788.
[142] S.M.M. Ramos, N. Bonardi, B. Canut, S. Bouffard and S. Della-Negra // *Nucl. Instr. Meth. B* **143** (1998) 319.
[143] M. Döbeli, F. Ames, C.R. Musil, L. Scandella, M. Suter and H.A. Synal // *Nucl. Instr. Meth. B* **143** (1998) 503.
[144] L.T. Chadderton // *Rad. Measurem.* **36** (2003) 13.
[145] S.A. Cruz, E.G. Gamaly, L.T. Chadderton and D. Fink // *Rad. Measurem.* **36** (2003) 145.
[146] T. Aoki, J. Matsuo and G. Takaoka // *Nucl. Instr. Meth. B* **202** (2003) 278.
[147] M. Henkel and H.M. Urbassek // *Nucl. Instr. Meth. B* **145** (1998) 503.
[148] T. Aoki, J. Matsuo and G. Takaoka // *Mat. Res. Soc. Symp. Proc.* **669** (2001) J4.5.1.
[149] J.-Y. Jin, J. Liu, P.A.W. van der Heide and W.-K. Chu // *Appl. Phys. Lett.* **76** (2000) 574.
[150] M. Döbeli, P.W. Nebiker, R. Mühle and M. Suter // *Nucl. Instr. Meth. B* **132** (1997) 571.
[151] D.A. Thompson // *J. Appl. Phys*. **52** (1981) 982.
[152] Z. Insepov and I. Yamada // *Nucl. Instr. Meth. B* **153** (1999) 199.
[153] J. Matsuo, N. Toyoda, M. Akizuki and I. Yamada // *Nucl. Instr. Meth. B* **121** (1997) 459.
[154] Y. Kitazoe and Y. Yamamura // *Rad. Eff. Lett.* **50** (1980) 39.
[155] M. Moseler, O. Rattunde, J. Nordiek and H. Haberland // *Nucl. Instr. Meth. B* **164-165** (2000) 522.
[156] N. Toyoda, H. Kitani, N. Hagiwara, J. Matsuo and I. Yamada // *Mater. Chem. Phys.* **54** (1998) 106.
[157] W. Christen and U. Even // *J. Phys. Chem. A* **102** (1998) 9420.
[158] T. Raz and R.D. Levine, In: *Chemical Dynamics in Extreme Environments,* ed. by R.A. Dressler (World Sci., Singapur, 2001) p. 20.
[159] W. Christen and U. Even // *Eur. Phys. J. D* **9** (1999) 29.
[160] H. Yasumatsu and T. Kondow // *Rep. Prog. Phys.* **66** (2003) 1783.
[161] M.H. Shapiro and T.A. Tombrello // *Phys. Rev. Lett.* **68** (1992) 1613.
[162] U. Even, I. Schek and J. Jortner // *Chem. Phys. Lett.* **202** (1993) 303.
[163] E. Hendel and U. Even // *J. Chem. Phys*. **103** (1995) 9045.
[164] U. Even, P.J. de Lange, H.Th. Jonkman and J. Kommandeur // *Phys. Rev. Lett.* **56** (1986) 965.
[165] Y. Le Beyec // *Int. J. Mass Spectrom. Ion Process*. **174** (1998) 101.
[166] E. Parilis // *Phys. Scripta* **68** (2003) C33.
[167] K.L. Merkle and W. Jäger // *Philos. Mag. A* **44** (1981) 741.
[168] I.H. Wilson, N.J. Zheng, U. Knipping and I.S.T. Tsong // *Phys. Rev. B* **38** (1988) 8444.
[169] I.H. Wilson, N.J. Zheng, U. Knipping and I.S.T. Tsong // *Appl. Phys. Lett.* **53** (1988) 2039.
[170] R. Neumann // *Nucl. Instr. Meth. B* **151** (1999) 42.

[171] C. Teichert, M. Hohage, T. Michely and G. Comsa // *Phys. Rev. Lett.* **72** (1994) 1682.
[172] F. Seitz and J.S. Koehler, In: *Solid State Physics: Advances in Research and Applications*, ed. by F. Seitz and D. Turnbull, Vol. 2 (New York: Academic, 1956) p. 305.
[173] R.S. Averback, T. de la Rubia, H. Hsieh and R. Benedek // *Nucl. Instr. Meth. B* **59/60** (1991) 709.
[174] Z. Insepov and I. Yamada // *Nucl. Instr. Meth. B* **112** (1996) 16.
[175] Y. Yamaguchi and J. Gspann // *Phys. Rev. B* **66** (2002) 155408.
[176] E.E. Zhurkin and A.S. Kolesnikov // *Nucl. Instr. Meth. B* **202** (2003) 269.
[177] G. Bräuchle, S. Richard-Schneider, D. Illig, J. Rockenberger, R.D. Beck and M.M. Kappes // *Appl. Phys. Lett.* **67** (1995) 52.
[178] L.P. Allen, D.B. Fenner, C. Santeufemio, W. Brooks, J. Hautala and Y. Shao // *Proceedings of SPIE* **4806** (2002) 225.
[179] R.C. Birtcher, A.W. McCormick, P.M. Baldo, N. Toyoda, I. Yamada and J. Matsuo // *Nucl. Instr. Meth. B* **206** (2003) 851.
[180] Z. Insepov, L.P. Allen, C. Santeufemio, K.S. Jones and I. Yamada // *Nucl. Instr. Meth B* **202** (2003) 261.
[181] A. Gruber and J. Gspann // *J. Vac. Sci. Technol. B* **15** (1997) 2362.
[182] J.-H. Song and W.-K. Choi // *Nucl. Instr. Meth. B* **190** (2002) 792.
[183] V.N. Popok, V.S. Prasalovich and E.E.B. Campbell // *Nucl. Instr. Meth. B* **207** (2003) 145.
[184] J.C. Giard, A. Michel, C. Tromas, C. Jaouen and S. Della-Negra // *Nucl. Instr. Meth. B* **209** (2003) 85.
[185] M. Toulemonde, C. Trautmann, E. Balanzat, K. Hjort and A. Weidinger // N*ucl. Instr. Meth. B* **216** (2004) 1.
[186] A. Audouard, R. Mamy, M. Toulemonde, G. Szenes and L. Thome // *Europhys. Lett.* **40** (1997) 527.
[187] V.A. Skuratov, D.L. Zagorski, A.E. Efimov, V.A. Kluev, Yu.P. Toporov and B.V. Mchedlishvili // *Radiat. Measur*. **34** (2001) 571.
[188] C. Müller, M. Cranney, A. El-Said, N. Ishikawa, A. Iwase, M. Lang and R. Neumann // *Nucl. Instr. Meth. B* **191** (2002) 246.
[189] V.A. Skuratov, S.J. Zinkle, A.E. Efimov and K. Havancsak // *Surf. Coat. Technol.* **196** (2005) 56.
[190] V.N. Popok, S.V. Prasalovich and E.E.B. Campbell // *Surf. Sci.* **566-568** (2004) 1179.
[191] V.N. Popok, S.V. Prasalovich and E.E.B. Campbell // *Vacuum* **76** (2004) 265.
[192] J.F. Ziegler, *The stopping and range of ions in matter* (SRIM-2003) <www.srim.org>
[193] M. Ghaly and R.S. Averback // *Phys. Rev. Lett.* **72** (1994) 364.
[194] S.G. Mayr, Y. Ashkenazy and R.S. Averback // *Nucl. Instr. Meth. B* **212** (2003) 246.
[195] R. Krämer, Y. Yamaguchi and J. Gspann // *Surf. Interface Anal.* **36** (2004) 148.
[196] J. Samela and K. Nordlund // private communication.
[197] G.S. Collins, H.J. Melosh, J.V. Morgan and M.R. Warner // *Icarus* **157** (2002) 24.
[198] M.D. Bjorkman and K.A. Holsapple // *Int. J. Impact Engng* **5** (1987) 155.
[199] V.N. Popok, S.V. Prasalovich, P. Persson and E.E.B. Campbell // *Eur. Phys. J. D* **36** (2005) 79.